Experimental study of heavy flavour production at RHIC and LHC

M. Biasini[a], *C. Bombonati*[b], *G.E. Bruno*[c], *E. Lytken*[d], *A. Mischke*[e], *C. Rosemann*[f], *A. Starodumov*[g,*], *D. Stocco*[h], *R. Wolf*[f], *and M. zur Nedden*[i]

[a] University and INFN, Perugia, Italy
[b] University and INFN, Padua, Italy
[c] University and INFN, Bari, Italy
[d] CERN, Geneva, Switzerland
[e] Institute for Subatomic Physics, Faculty of Science, Utrecht University, Utrecht, the Netherlands
[f] Inst. für Experimentalphysik, Universität Hamburg and DESY, Germany
[g] Paul Scherrer Institut, PSI Villigen, Switzerland
[h] University and INFN, Torino, Italy
[i] Humboldt-University of Berlin, Germany

Abstract

After reviewing the main heavy flavour results from experiments at the Relativistic Heavy Ion Collider (RHIC), we present the expected performance for some of the most significative measurements in the heavy flavour sector at the Large Hadron Collider (LHC), for the experiments ALICE, ATLAS, and CMS.

Coordinator: A. Dainese

1 Heavy flavour physics at RHIC

Author: A. Mischke

1.1 Introduction

Measurements at RHIC have revealed strong modification of the jet structure in high-energy nuclear collisions due to the interaction of hard scattered partons with the hot and dense medium created in these reactions. The study of heavy-quark (charm and bottom) production in the medium offers unique opportunities for the investigation of the properties of the Quark-Gluon Plasma (QGP). Heavy quarks are believed to be produced predominantly in hard scattering processes in the early stage of the collision, and they probe the produced medium as they propagate through it [1]. Due to their higher mass, the penetrating power is much higher for heavy quarks than for light quarks, providing a sensitive probe of the medium. The energy loss of heavy quarks in the medium is expected to be smaller compared to light quarks due to the mass dependent suppression of the gluon radiation under small angle, known as the dead-cone effect [2, 3].

*On leave from ITEP, Moscow, Russia

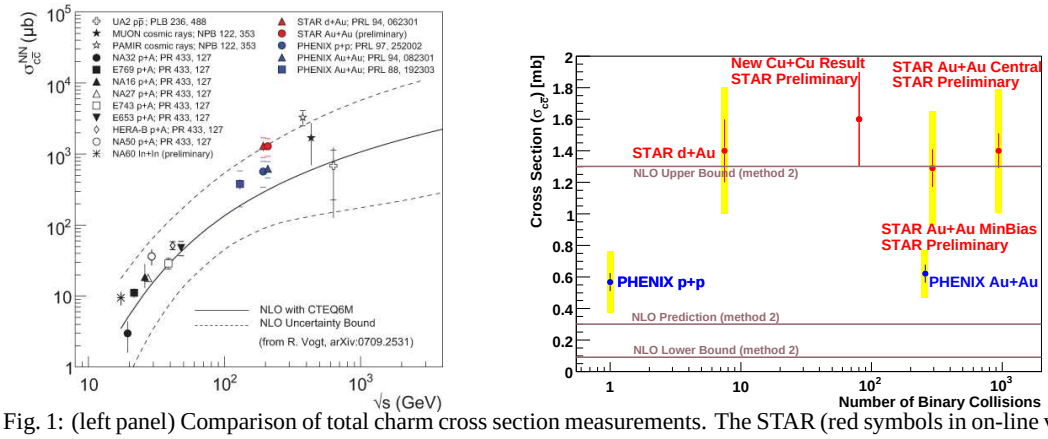

Fig. 1: (left panel) Comparison of total charm cross section measurements. The STAR (red symbols in on-line version) and PHENIX results (blue symbols in on-line version) are given as cross section per binary collisions. The dashed curves depict the uncertainty bands of the NLO calculations. (right panel) Total charm cross section divided by the number of binary collisions for different collisions systems, compared to NLO calculations (horizontal lines).

1.2 Total charm cross section

The total charm cross section is currently determined through basically three different measurements: direct reconstruction of D mesons, muons and electrons. Electron identification in the PHENIX experiment is based on the Ring Imaging Cherenkov detector (RICH) in conjunction with a highly granular calorimeter. The particle momentum is measured by drift and pad chambers. The subtraction of the electron background (mainly from photons, π^0 and η) is performed by the converter and the cocktail methods [4, 5], which give similar results. In the STAR experiment, electrons are identified using the dE/dx and momentum measurements from the TPC together with the Time of Flight (ToF) information at low $p_{\rm T}$ ($< 4-5$ GeV/c) and energy (E) and shower shape measurement in the electromagnetic calorimeter (EMC) at high-$p_{\rm T}$ (> 1.5 GeV/c). The background contribution to the electrons from photonic sources are subtracted statistically [6].

The total charm cross section is extracted from a combined fit to the measured particle spectra. The STAR data are from combined fits to hadronic and semileptonic decay data. The PHENIX data are from semileptonic decay measurements only. The total cross sections from STAR and PHENIX are compared to results at other energies and to NLO calculations [7] in Fig. 1 (left panel). The descrepancy between STAR and PHENIX is under investigation. The data agree with the NLO prediction on the total charm cross section. The large theoretical uncertainty leads to a little predictive power in the total charm cross section. Fig. 1 (right panel) depictes the charm cross section divided by the number of binary collisions for different collisions systems. Within errors, the charm cross section for the different collisions systems follows binary collisons scaling, supporting the assumption that charm is predominantely produced by hard scattering in the initial state of the collision.

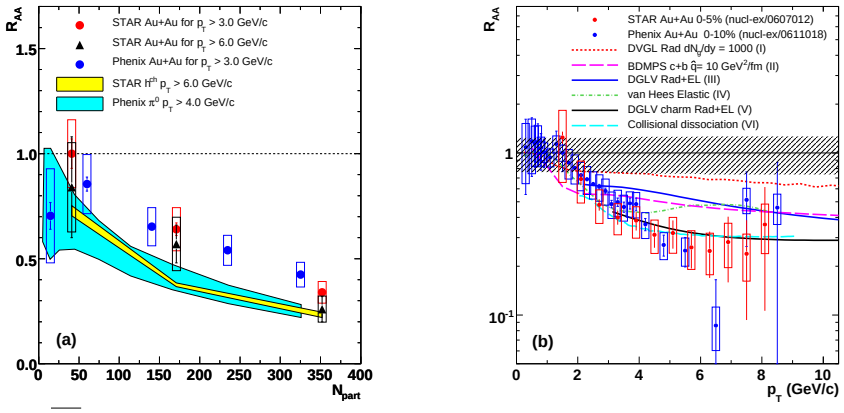

Fig. 2: Nuclear modification factor R_{AA} of non-photonic electrons in Au+Au collisions. (a) R_{AA} as a function of N_{part}. (b) R_{AA} as a function of $p_{\rm T}$ for the most central collisions.

1.3 Heavy-quark energy loss in hot and dense QCD matter

Nuclear effects are typically quantified using the nuclear modification factor R_{AA} where the particle yield in Au+Au collisions is divided by the yield in pp reactions scaled by the number of binary collisions. $R_{AA} = 1$ would indicate that no nuclear effects, such as Cronin effect, shadowing or gluon saturation, are present and that nucleus-nucleus collisions can be considered as a incoherent superposition of nucleon-nucleon interactions. The average R_{AA} for high-$p_{\rm T}$ non-photonic electrons as a function of participating nucleons (N_{part}) is illustrated in Fig. 2(a). The STAR and PHENIX R_{AA} for non-photonic electrons are consistent with each other and shows an increasing suppression from peripheral to central Au+Au collisions, indicating an unexpectedly energy loss of heavy quarks in the medium in contradiction to expections from the dead-cone effect. The suppression is similar to the one observed for light-quark hadrons, indicated by the shaded area in the figure. Fig. 2(b) shows the $p_{\rm T}$ dependence R_{AA} of non-photonic electrons in central Au+Au collisions. A strong suppression of a factor of ~ 5 is observed for $p_{\rm T} > 6$ GeV/c. The R_{AA} is compared to several theoretical model calculations [4, 6]. The observed suppression is overpredicted by the models using reasonalbe model parameters. The data is described reasonably well if the bottom contribution to the electrons is assumed to be small. Therefore, the observed discrepancy could indicate that the B dominance over D mesons starts at higher $p_{\rm T}$. A possible scenario for B meson suppression invokes collisional dissociation in the medium.

1.4 Heavy-quark azimuthal correlations

The measurement of the relative charm and bottom contributions to the non-photonic electrons is essentail for the interpretation of the non-photonic electron spectra. Azimuthal angular correlations between non-photonic electrons and hadrons allow to indentify the underlying production process [8]. Heavy flavours have, in general, a harder fragmentation function than gluons and light quarks, making the near-side correlation more sensitive to the decay kinematics. For the same electron transverse momentum the near-side $e-$hadron angular correlation from B decays is much broader than that from D decays. Fig. 3 (left panel) shows the azimuthal correlation

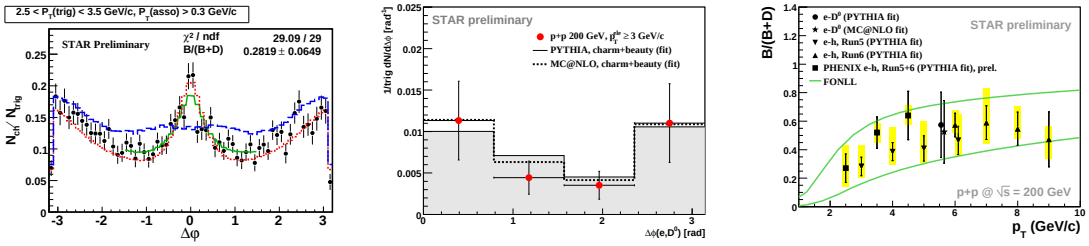

Fig. 3: (left panel) $e-$hadron azimuthal correlation distribution in 200 GeV pp collisions, compared to PYTHIA simulations (colored curves). (middle panel) $e-D^0$ azimuthal correlation distribution for like-sign $e-K$ pairs. The grey histogram (dashed line) illustrates results from PYTHIA (MC@NLO) simulations. (right panel) Relative bottom contribution to the total non-photonic electron yield derived from e$-D^0$ and e$-$hadron correlations, compared to the uncertainty band from a FONLL calculation.

function of non-photonic electrons and hadrons in pp collisions at $\sqrt{s}$ = 200 GeV. The data is fitted with a linear combination of the simulated charm and bottom distribution, obtained from PYTHIA simulations, to extract the relative bottom contribution $B/(B+D)$. Similar studies are performed for $e-D^0$ azimuthal correlations [8] (cf. Fig. 3, middle panel). Moreover, it has been shown that higher order sub-processes like gluon splitting may have a significant contribution to the near-side correlation. This contribution is studied by indentifying the D* content of jets [8]. The results indicate that gluon splitting to $c\bar{c}$ pairs contributes about 5% of the open charm production observed at RHIC, consistent with predictions from MC@NLO calculations [9].

The relative bottom contribution $B/(B+D)$ is shown in Fig. 3 (right panel) together with predictions from FONLL calculations [10]. These data provide convincing evidence that bottom contributes significantly ($\sim 50\%$) to the non-photonic electron yields at high-$p_{\rm T}$. Further studies have to show whether these findings imply substantial energy loss of bottom quarks in the produced medium.

1.5 Summary and conclusions

The measured total charm cross section follows binary collisions scaling as expected from the assumption that charm is produced exclusively in initial hard scattering processes. The high-$p_{\rm T}$ suppression of the non-photonic electron yield in Au+Au collisions is much larger than expected. Theoretical explanations are yet inconclusive. The bottom contribution in the non-photonic electron spectrum is studied by $e-$hadron and $e-D^0$ correlations. First measurements on the charm content in jets shows that the gluon splitting contribution is small at RHIC. Detailed and systematic studies will be possible with heavy flavour measurements in the ALICE experiment at the CERN-LHC [11].

Acknowledgments
The author thanks the organizers for the stimulating atmosphere during the workshop. This work is supported by a Veni grant from the Netherlands Organization for Scientific Research (project number: 680-47-109).

2 Heavy flavour program of the ALICE experiment at the LHC

Authors: C. Bombonati, G.E. Bruno, and D. Stocco

2.1 Introduction

The Large Hadron Collider (LHC) will produce proton–proton, Pb–Pb , other lighter systems like Ar–Ar and proton induced nucleus collisions up to the energies corresponding to the maximum magnetic rigidity of $23,350\,\mathrm{Tm}$ (e.g., proton–proton and Pb–Pb collisions at centre-of-mass energy per nucleon–nucleon $\sqrt{s_{\mathrm{NN}}} = 14\,\mathrm{TeV}$ and $5.5\,\mathrm{TeV}$, respectively). ALICE [12, 13] is the dedicated heavy-ion experiment at the LHC; its main physics goal is the study of strongly-interacting matter in the conditions of high-energy density ($> 10\,\mathrm{GeVfm}^{-3}$) and high temperature ($\gtrsim 0.2\,\mathrm{GeV}$) over large volume ($10^2$–$10^3$ fm^3), expected to be reached in central Pb–Pb collisions. The ALICE apparatus [12, 13] has excellent capabilities for heavy-flavour measurements, for both open heavy-flavoured hadrons and quarkonia. In this paper, we shall limit the discussion to the detection of open charm and beauty in the central barrel (section 2.2) and of quarkonium states at forward rapidity (section 2.4), with an emphasis on the proton–proton collisions. Therefore only the detectors involved in these analyses are described in the following.

The ALICE central barrel covers the pseudo-rapidity region $-0.9 < \eta < 0.9$ and is equipped with tracking detectors and particle identification systems embedded in a magnetic field $B = 0.5$ T. The combined information from the central barrel detectors allows to track charged particles down to low transverse momenta (low p_{T} cut-off $\approx$ 100 MeV/c) and provides hadron and electron identification as well as an accurate measurement of the positions of the primary (interaction) vertex and of the secondary (decay) vertices. The main tracking detector is the Time Projection Chamber (TPC) which provides track reconstruction and particle identification via $\frac{dE}{dx}$. The Inner Tracking System (ITS) is the innermost central barrel detector and is composed of six cylindrical layers of silicon detectors. The two layers closest to the beam pipe (at radii of $\approx$ 4 and 7 cm) are equipped with pixel detectors, the two intermediate layers (radii $\approx$ 15 and 24 cm) are made of drift detectors, while strip detectors are used for the two outermost layers (radii $\approx$ 39 and 44 cm). The ITS is a key detector for open heavy-flavour studies because it allows to measure the track impact parameter (i.e. the distance of closest approach of the track to the primary vertex) with a resolution better than 50 μm for $p_{\mathrm{T}} > 1.3\,\mathrm{GeV}/c$, thus providing the capability to detect the secondary vertices originating from heavy-flavour decays. Two other systems play an important role in the heavy-flavour analyses as far as particle identification is concerned. They are the Transition Radiation Detector (TRD) for high-momentum electron identification and the Time-Of-Flight (TOF) for pion, kaon and proton separation. All these four detectors have full azimuthal coverage.

The detection of heavy quarkonia in the di-muonic decay channel is performed by the ALICE Muon Spectrometer in the forward pseudo-rapidity region $2.5 < \eta < 4$. The detector consists of five tracking stations with two planes of Multi-Wire Proportional Chambers each, with a spatial resolution of about 100 μm, a dipole magnet with an integral field of 3 Tm and two trigger stations of Resistive Plate Chambers placed behind an iron-wall muon filter with a thickness of about 7 interaction lengths. The system is completed by a front absorber of composite material, predominantly made of carbon and concrete, which is placed at 90 cm from the

interaction vertex to reduce the free decay length of pions and kaons, and a beam shield made of tungsten, lead and stainless steel to protect the chambers from particles and secondaries produced at large rapidities. The spectrometer can detect quarkonia down to $p_{\rm T} = 0$ and is designed to achieve an invariant-mass resolution of 70 (100) MeV/c^2 at 3 (10) GeV/c^2, needed to resolve the J/ψ (Υ) resonances.

2.2 Open heavy flavour in the ALICE Central Barrel

Heavy flavours are produced in initial parton-parton interactions, in the early stage of the collision. Their production can be calculated to a reasonable degree of precision within pQCD and they offer the possibility to explore the properties of the medium created in the collision with probes of known mass and colour charge. The energy loss by gluon radiation, for instance, is expected to be parton-specific (stronger for gluons than for quarks due to the larger colour charge of gluons) and flavour-specific (stronger for lighter than for heavier quarks, due to the dead cone effect [14, 15]). In addition, the measurement of open heavy-flavour production is of an essential practical interest for quarkonium physics as well, both as a natural reference and B meson decays being a sizable source of non-prompt J/ψ in high energy collisions.

In figure 4 we compare schematically the ALICE $p_{\rm T}$ vs. η acceptance for charm (c) and beauty (b) hadrons to that of the other LHC experiments, for proton–proton collisions at $\sqrt{s} = 14$ TeV. In this plot the high $p_{\rm T}$ reach is the one expected for one year of running at nominal luminosity (note that the value of the luminosity is different for each experiment: 10^{34} cm^{-2}s^{-1} for ATLAS and CMS, 2–5$\times 10^{32}$ cm^{-2}s^{-1} for LHCb, and 3×10^{30} cm^{-2}s^{-1} for ALICE). ATLAS and CMS have similar acceptance for beauty measurements. On one hand, their minimum accessible $p_{\rm T}$ is larger than for ALICE because of the strong magnetic fields and the larger material budget in the inner tracking detectors; on the other hand, the strong magnetic fields, together with the high luminosity, allow those experiments to cover transverse momenta up to 200–300 GeV/c. In terms of acceptance for beauty measurements, ALICE overlaps with ATLAS and CMS at central rapidity and with LHCb at forward rapidity. The moderate magnetic field allows measurements down to transverse momenta of less than 1 GeV/c for charmed and beauty hadrons in the central barrel[1].

For the performance study presented here, we assume the baseline heavy-flavour production cross sections and yields presented in the ALICE Physics Performance Report,Volume II [13]. Those values are obtained from the pQCD calculations at fixed next-to-leading-order (FO NLO) implemented in the HVQMNR program [16]; note that the cross sections have a theoretical uncertainty of about a factor 2 [13].

2.2.1 Exclusive charm meson reconstruction

Among the most promising channels for open charm detection are the $\rm D^0 \rightarrow K^-\pi^+$ ($c\tau \approx 120$ μm, branching ratio $\approx 3.8\%$) and $\rm D^+ \rightarrow K^-\pi^+\pi^+$ ($c\tau \approx 300$ μm, branching ratio $\approx 9.2\%$) decays. The detection strategy to cope with the large combinatorial background from the underlying event in Pb–Pb is based on the selection of displaced-vertex topologies [13,

[1]The study of the channel $B \rightarrow$ J/$\psi + X$, discussed in section 2.3, should allow a determination of the $p_{\rm T}$ differential cross section of B hadrons down to $p_{\rm T} \approx 0$.

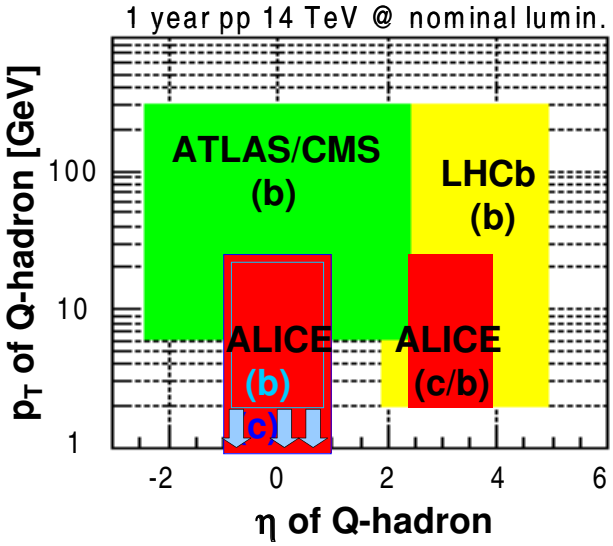

Fig. 4: Schematic acceptance in transverse momentum and pseudorapidity for open heavy flavour hadrons (indicated as Q-hadrons) in the four LHC experiments. The high-$p_{\rm T}$ coverages correspond to one year (i.e. 7 months) of running at nominal luminosity.

17]. An invariant-mass analysis is used to extract the raw signal yield, to be then corrected for selection and reconstruction efficiency and for detector acceptance. As shown in figure 5 (left), the accessible $p_{\rm T}$ range for the $\rm D^0$ is 1–20 GeV/c in Pb–Pb and 0.5–20 GeV/c in proton–proton, with statistical errors better than 15–20% at high $p_{\rm T}$. A similar performance is expected for the $\rm D^+$ (right-hand panel), though at present the statistical errors are estimated only in the range $1 < p_{\rm T} < 8$ GeV/c. The systematic errors (acceptance and efficiency corrections, centrality selection for Pb–Pb) are estimated to be smaller than 15%.

2.2.2 Beauty detection via displaced electrons

Beauty detection via electron-identified tracks with a displacement with respect to the primary collision vertex is favoured by the large semi-electronic branching ratio (b.r. $\approx 11\%$ [18]) and by the significant mean proper decay length ($c\tau \approx 500$ μm [18]) of beauty hadrons. The main sources of background for the signal of beauty-decay electrons are: decays of primary D mesons, which have a branching ratio of $\approx 10\%$ in the semi-electronic channels [18], and have an expected production yield larger by a factor about 20 with respect to B mesons ($N^{c\overline{c}} \approx 1.6 \times 10^{-1}$/ev and $N^{b\overline{b}} \approx 7.2 \times 10^{-3}$/ev [13]); di-electron decays of vector mesons (ρ, ω, ϕ) and Dalitz decays of pion and η mesons (e.g., $\pi^0 \rightarrow \gamma e^+ e^-$); conversions of photons in the beam pipe or in the inner layers of the ITS; charged pions misidentified as electrons.

Events were generated using PYTHIA [19]. We evaluated the required statistics at about 10^7 proton–proton minimum-bias events at $\sqrt{s} = 14$ TeV, 10^6 proton–proton events containing a

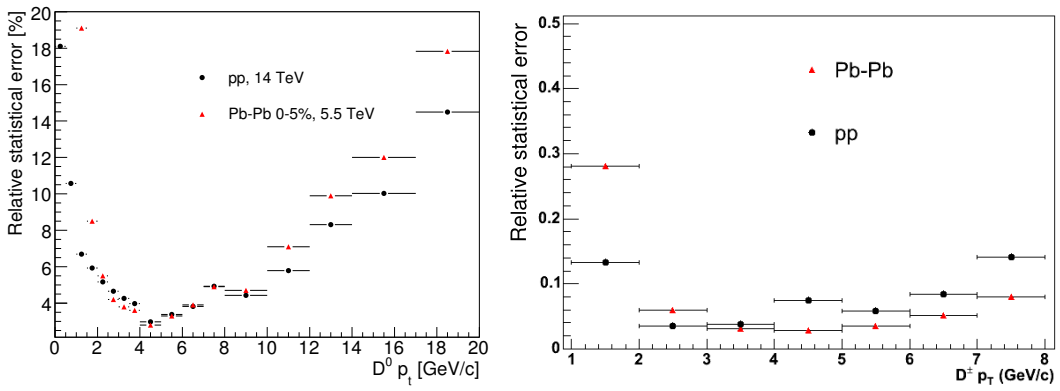

Fig. 5: Expected relative statistical errors for the measurement in ALICE of the production cross sections of D^0 in the $\mathrm{K}^-\pi^+$ channel (left) and D^+ in the $\mathrm{K}^-\pi^+\pi^+$ channel (right), in 0–5% central Pb–Pb collisions and in proton–proton collisions.

$c\overline{c}$ pair and 10^6 proton–proton events containing a $b\overline{b}$ pair. For the background, we used a sample of 6×10^6 minimum-bias proton–proton events. For the proton–proton events with a heavy-quark pair, we used the same PYTHIA settings as for the minimum-bias events, without forcing heavy-flavour production, but selecting events containing a $c\overline{c}$ or $b\overline{b}$ pair (in oder to obtain a realistic underlying-event multiplicity). Since the resulting shapes of the charm and beauty quarks p_{T} distributions are different from those given by NLO pQCD predictions [16] we reweighted the decay electrons in order to match the baseline shapes. The samples, for background and for proton–proton events with a heavy-quark pair, were normalized to one proton–proton event.

Figure 6 shows the distributions of the signal and of the different background sources, in impact parameter, defined in the plane transverse to the beam direction, (d_0) and in transverse momentum (p_{T}). The detection strategy is adapted from that developed for Pb–Pb collisions [20] and is based on three steps:

1. Electron identification. Electrons can be efficiently separated from hadrons by combining the PID capabilities of the TPC, and of the TRD. Here we assume for the proton–proton case the same electron PID performance as expected in Pb–Pb collisions [20]. Under the assumption of $e_{eff}^{TRD} = 90\%$ electron identification probability, the TRD is expected to reject 99% of the charged pions ($\pi_{eff}^{TRD} = 10^{-2}$ misidentification probability) and fully reject heavier charged hadrons, for $p > 1$ GeV/c. Using the information from the TPC, the probability of pion misidentification can be further reduced by a factor of a hundred at low momentum. As the momentum increases and charged pions approach the Fermi plateau in $\frac{dE}{dx}$, the additional pion rejection from the TPC decreases and becomes marginal at $p \simeq 10$ GeV/c.
2. Primary vertex reconstruction. Due to the TPC and SDD drift speed limitations, during LHC proton–proton runs, the luminosity at the ALICE interaction point has to be kept below $\mathcal{L}_{max} \simeq 3\times10^{30}\ \mathrm{cm}^{-2}\mathrm{s}^{-1}$ [12]. When the LHC luminosity will be larger than this value (the design luminosity is about a factor 10^4 higher), the luminosity at the ALICE

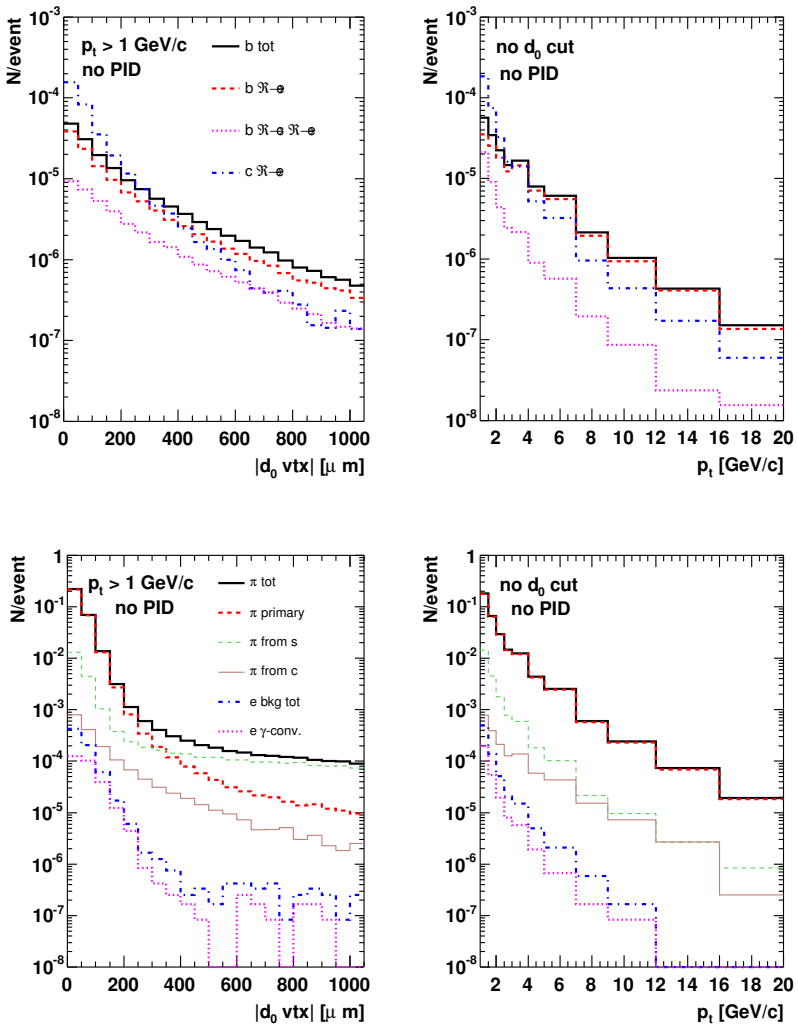

Fig. 6: Beauty and charm decay electrons (top), electrons from other sources and charged pions (bottom), as a function of $|d_0|$ (left) and $p_{\rm T}$ (right). Here, $|d_0|$ is calculated with respect to the true primary vertex position, known from simulation.

interaction point will have to be reduced, for instance by defocusing the beams, i.e. by enlarging their transverse size up to $\sigma_{x,y} \sim 150$ μm. The primary vertex position will be reconstructed on an event-by-event basis, using measured tracks, with an expected resolution of about 70 μm in x and y on average [21].

3. Impact parameter cut. Because of the large mean proper decay length (≈ 500 μm) of beauty mesons, their decay electrons have a typical impact parameter of a few hundred microns with respect to the primary vertex. A cut $|d_0| \gtrsim 200$ μm allows to reject a large fraction of the background (see Fig. 6). We have optimized the value of this cut as a

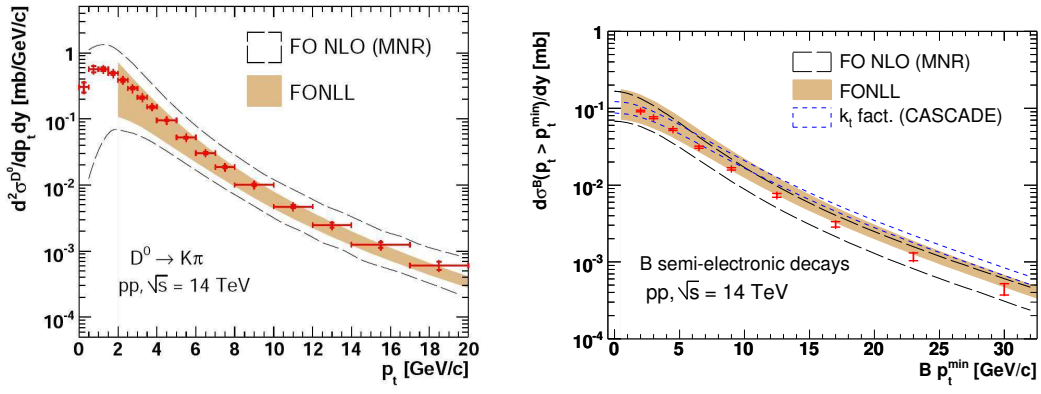

Fig. 7: Differential cross section for D^0 (left) and B meson (right) production as it can be measured with 10^9 p–p minimum-bias events. Statistical errors (inner bars) and quadratic sum of statistical and p_{T}-dependent systematic errors (outer bars) are shown; the 9% normalization error is not shown. The theoretical predictions from the three pQCD calculations (see text), with their uncertainties are also shown for comparison with the expected experimental sensitivity.

function of the transverse momentum in order to minimize the total errors (statistical and systematic).

To extract the electrons cross section we first apply our cuts to the "measured" electrons. On this selected sample we subtract the residual background (estimated from the charm and pions measurements) and we apply the corrections for efficiency and acceptance. We infer the p_{T}^{min}-differential cross section for beauty mesons, $d\sigma^B(p_{\mathrm{T}} > p_{\mathrm{T}}^{min})/dy$, from the beauty electrons cross section using a procedure similar to that developed by the UA1 Collaboration [22]. The method, described in detail in Refs. [13, 20, 23], is based on Monte Carlo simulation and relies on measured B meson decay kinematics.

2.2.3 Results

Figure 7 presents the expected ALICE performance for the measurement of the p_{T}-differential cross section of D^0 mesons (left) and the p_{T}^{min}-differential cross section of B mesons, $d\sigma^B(p_{\mathrm{T}} > p_{\mathrm{T}}^{min})/dy$ vs. p_{T}^{min} averaged in the range $|y| < 1$. For illustration of the sensitivity in the comparison to pQCD calculations, we report in the same figure the predictions and the theoretical uncertainty bands from three approaches [24]: collinearly-factorized FO NLO, as implemented in the HVQMNR code [16], Fixed Order Next-to-Leading Log (FONLL) [25] and k_t-factorization, as implemented in the CASCADE code [26]. It can be seen that the expected ALICE performance for 10^9 events will provide a meaningful comparison with pQCD predictions.

2.3 Beauty in the J/ψ channel

Simulation studies are in progress to prepare a measurement of the fraction of J/ψ that feed-down from B decays. Such measurement can be performed by studying the separation of the dilepton

pairs in the J/ψ invariant-mass region from the main interaction vertex. The analysis should provide a measurement of the beauty $p_{\rm T}$-differential cross section down to $p_{\rm T} \approx 0$. The pseudo-proper decay time, $x = L_{xy} \cdot M(\rm J/\psi)/p_{\rm T}$, where L_{xy} is the signed projection of the J/ψ flight distance on its transverse direction, $L_{xy} = \vec{L} \cdot \vec{p}_{\rm t}(\rm J/\psi)/|p_{\rm T}|$, can be used to separate J/ψ from the B decay products from that of prompt decays, as shown in figure 8 for proton–proton collisions. In this expression, the $M(\rm J/\psi)$ is taken as the known J/ψ mass [18].

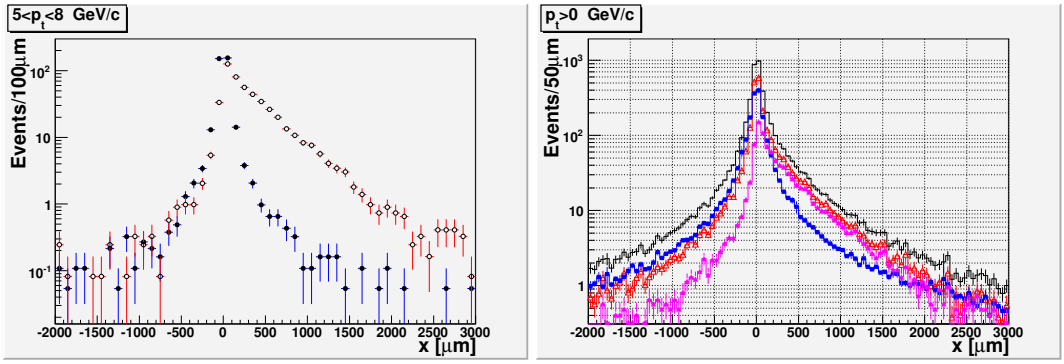

Fig. 8: Distributions of the x variable, defined in the text, for $5 < p_{\rm T} < 8$ GeV/c (left) showed for secondary (open circles) and prompt (closed circles) J/ψ, and for $p_{\rm T} > 0$ (right) showed for total J/ψ (open triangles), secondary J/ψ (closed triangles), total background (closed squares) and their sum (lines, in black).

2.4 Quarkonia detection in the ALICE Muon Spectrometer

The ALICE experiment will detect heavy quarkonia both at central rapidity in the di-electronic decay channel and at forward rapidity in the di-muonic one. The latter channel will be discussed here.

Quarkonia cross sections at LHC energies are provided by the Color Evaporation Model (CEM) [27]. In this model, the quarkonia cross section is the product of the $\rm Q\overline{Q}$ cross section times a transition probability (F_C) which is specific to each state (C) but independent of the energy. Ground state cross sections are the sum of direct production and feed-down from higher mass resonances below the thresholds for heavy-flavoured meson production (H = B or D). At leading order:

$$\sigma_C^{CEM} = F_C \sum_{i,j} \int_{4m_Q^2}^{4m_H^2} {\rm d}\hat{s} \int {\rm d}x_1 {\rm d}x_2 \, f_{i/A}(x_1,\mu^2) f_{j/B}(x_2,\mu^2) \hat{\sigma}_{ij}(\hat{s}) \delta(\hat{s} - x_1 x_2 s) \qquad (1)$$

where A and B can be any hadron or nucleus, $ij = \rm q\overline{q}$ or gg, $\hat{\sigma}_{ij}(\hat{s})$ is the $ij \rightarrow \rm Q\overline{Q}$ subprocess cross section and $f_{i/A}(x_1,\mu^2)$ is the parton density in the hadron or nucleus. The predictions for proton–proton collisions at 14 TeV are summarized in Table 1. The transverse momentum distributions are obtained by extrapolating the distributions measured by the CDF experiment at $\sqrt{s} \sim 2$ TeV [28] at the LHC energies. The $p_{\rm T}$ and rapidity distributions of J/ψ and $\psi(2S)$ from

	J/ψ	$\psi(2S)$	Υ	$\Upsilon(2S)$	$\Upsilon(3S)$
$\sigma \times$ BR (μb)	3.18	0.057	0.028	0.007	0.0042

Table 1: CEM cross sections for quarkonia production in proton–proton collisions at 14 TeV. Cross sections include feed-down from higher mass resonances and branching ratios in lepton pairs.

the decay of B mesons are generated with PYTHIA [19]. The background, consisting in opposite sign dilepton pairs from the decay of charm, beauty, pions and kaons, is produced with PYTHIA as well.

The dimuon invariant-mass yield expected in one year of data taking in proton–proton collisions at the LHC, with a luminosity of 3×10^{30} cm^{-2}s^{-1} is shown in figure 9. The left (right) panel shows the results obtained with a trigger $p_{\rm T}$ cut of 1 (2) GeV/c in the J/ψ (Υ) mass region. About 2.8×10^6 J/ψ and 2.7×10^4 Υ are expected. The high statistics allows to reconstruct differential distributions with a fine binning, as illustrated in figure 10.

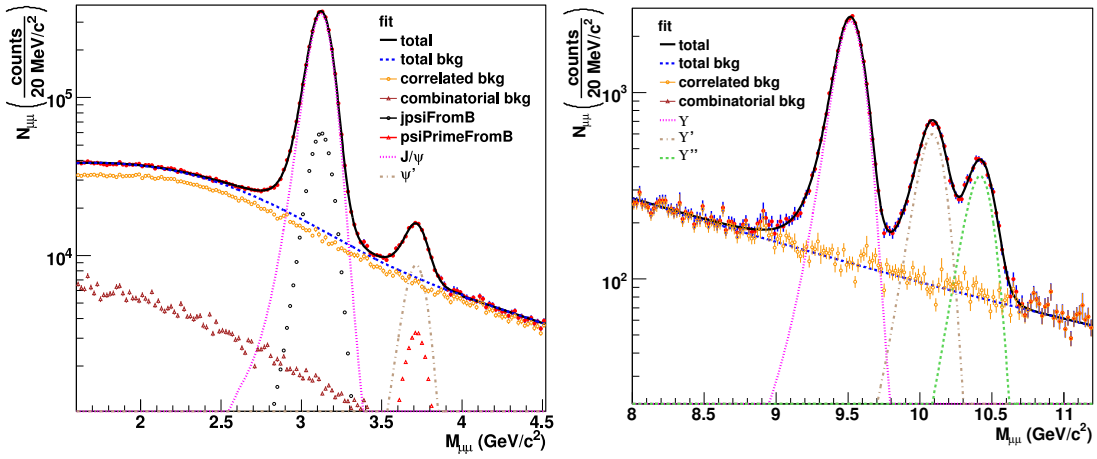

Fig. 9: Dimuon invariant-mass distribution expected in 1 year of data taking in proton–proton collisions at 3×10^{30} cm^{-2}s^{-1}.

2.4.1 Sensitivity to low x PDFs

The choice of a hadron collider implies some uncertainties in the determination of the initial state during the collisions, which are related to the composite nature of the colliding particles. At high energies the hadrons do not interact as a whole: the scatterings takes place between the constituent quarks and gluons. An accurate knowledge of the momentum distribution of such elementary particles in the hadrons is a fundamental issue. The mapped phase space is constantly increased by taking into account data from experiments at different energies. At present, the gluon distribution are constrained by measurements down to x values higher than 10^{-4}, and extrapolated down to about 10^{-5}.

Leading order calculations show that in proton–proton collisions at 14 TeV, the J/ψ with a rapidity higher than 3 are produced by gluons with $x < 10^{-5}$. Figure 11 shows a comparison

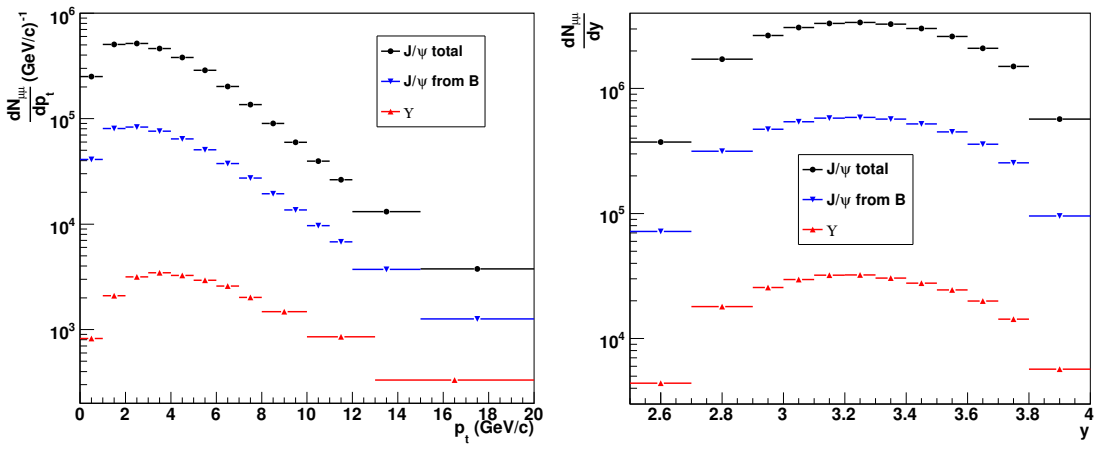

Fig. 10: Expected p_{T} (left panels) and rapidity (right panels) differential yields for J/ψ and Υ in 1 year of data taking in proton–proton collisions at 14 TeV at the ALICE nominal luminosity of 3×10^{30} cm^{-2}s^{-1}.

among the PDF sets calculated at Leading Order by the collaborations Martin-Roberts-Stirling-Thorne (MRST98 [29] and MRST01 [30]) and the Coordinated Theoretical-Experimental Project on QCD (CTEQ5 [31] and CTEQ6 [32]) at the scale of J/ψ (left panel) and Υ (right panel). For the MRST01 and CTEQ5 sets, two different extrapolations in the low x region are shown. Differently from the Υ case, the x-values explored by J/ψ in the ALICE Muon Spectrometer acceptance (in yellow), partially sit on the region of extrapolation.

Performing Leading Order calculations in the framework of the Color Evaporation Model,

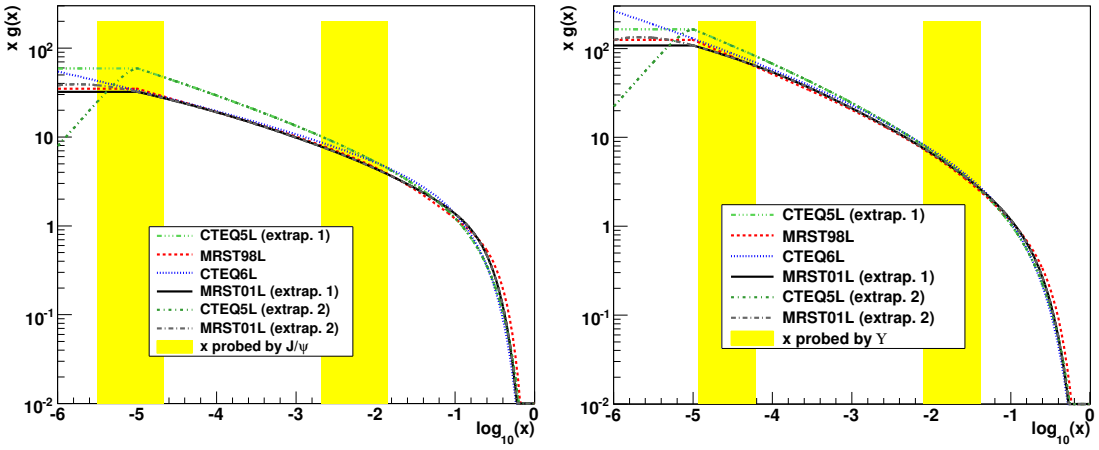

Fig. 11: Comparison of the gluon distributions from MRST and CTEQ. x regions probed by J/ψ and Υ produced in proton–proton collisions at $\sqrt{s} = 14$ TeV in the rapidity region $2.5 < y < 4$ are shown.

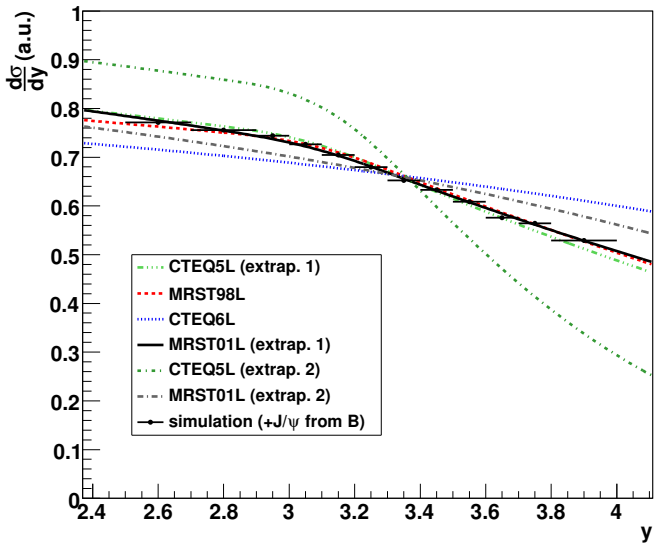

Fig. 12: Comparison between J/ψ rapidity distributions obtained with four different PDF sets (area in detector acceptance is normalized to 1). Simulation results are also shown.

it is possible to derive the J/ψ rapidity distribution:

$$\frac{\mathrm{d}\sigma^{CEM}_{\mathrm{J}/\psi}}{\mathrm{d}y} = \frac{F_{\mathrm{J}/\psi}}{s} \sum_{i,j} \int_{4m_Q^2}^{4m_H^2} \mathrm{d}\hat{s}\, \hat{\sigma}_{ij}(\hat{s}) f_{i/A}(\sqrt{\frac{\hat{s}}{s}} e^{y}, \mu^2) f_{j/B}(\sqrt{\frac{\hat{s}}{s}} e^{-y}, \mu^2) \qquad (2)$$

Figure 12 shows a comparison of the differential distributions obtained with different sets of PDFs. It is worth noting that such distributions are normalized by setting equal to unit their integral from 2.5 to 4 rapidity units. The *shape* of the distributions is clearly dependent on the behavior of the gluon functions: results obtained with MRST98L, MRST01L (extrap. 1) and CTEQ5L (extrap. 1), which were extrapolated flat in $xg(x)$ (figure 11) are compatible among each other and are clearly different from the result obtained with CTEQ6L, and with a changed extrapolation behavior of MRST01L (extrap. 2) and CTEQ5L (extrap. 2). The results show that also a small change in the PDFs extrapolation (see MRST01L) can lead to appreciable changes in the shape of the differential distributions.

The comparison between the simulation results and the calculations (figure 12), show that, due to the high statistics, the accuracy of the data expected to be collected by the ALICE Muon Spectrometer will be good enough to allow to discriminate among different shapes of the gluon distribution functions in the region of $x < 10^{-5}$ (at least in the frame of a leading order analysis).

2.5 Conclusions

We presented the expected performance of ALICE for the study of open heavy flavour and quarkonium states in nucleus–nucleus collisions at the LHC. Thanks to the good expected performace of the detectors for tracking and particle identification, and its low magnetic field in

the central barrel, the ALICE acceptance is complementary to that of other LHC experiments. This opens the possibility of measuring heavy-flavour production down to $p_{\rm T} \approx 1\,{\rm GeV}/c$, both at central and forward rapidity. Our results indicate that ALICE can provide several $p_{\rm T}$ differential measurements of charmed and beauty hadrons production with errors that are smaller or comparable to the theoretical uncertainties of pQCD calculations. The invariant-mass resolution of the muon spectrometer allows to resolve several charmonium and bottomonium resonances and the statistics expected to be collected in the first year of data taking should be enough to study in details the production of several quarkonia states. Finally, ALICE will probe the parton distribution functions down to unprecedentedly low values of the Feynman x variable.

3 Quarkonia and open beauty production in the ATLAS experiment at the LHC

Authors: E. Lytken and M. zur Nedden

3.1 Introduction

ATLAS [33] is a general-purpose experiment with main emphasis on searches for new phenomena based on high $p_{\rm T}$ particles. Since most of the B-physics appears in the lower $p_{\rm T}$ range, triggering within the LHC environment on those events is a challenge. Nevertheless, ATLAS has good capabilities for a rich B-physics program, based on the dedicated and flexible trigger, the precise and flexible vertexing and tracking, the good muon identification and the high-resolution calorimetry. Furthermore, theoretical descriptions of heavy flavoured hadrons need input from the LHC, where precision measurements are already achievable after one year of data taking. The expected inclusive production cross-section for $b\overline{b}$ pairs at LHC is estimated to be $\sigma_{b\overline{b}} \approx 500\ \mu{\rm b}$ leading to more than 10^6 produced pairs per second at design luminosity. The experimental precision reached at ATLAS should at least allow the verification of the Standard Model (SM) prediction. In the case of the rare B-decays, clearly higher luminosity is needed to achieve sensitive upper limits for the indirect beyond the Standard Model (BSM) searches. Therefore, the most relevant part of the ATLAS B-physics program will take place in the initial phase at lower luminosities with an extension into the high luminosity phase. The envisaged measurements are extending the discovery potential for physics beyond the SM by the measurement of CP violation parameters, predicted to be small in the SM, and of rare B decays.

The exclusive B^+ channel provides a clean reference signal. Due to the clear event topology and its rather large branching ratio, it can be measured during the initial luminosity phase of the LHC. The $B^+ \rightarrow J/\psi K^+$ decay can serve as a reference channel for the measurement of the decay probability of a very rare decay channel $B_s \rightarrow \mu^+\mu^-$, which is strongly suppressed in the Standard Model and therefore offers a good sensitivity to new physics. The total and differential cross-sections of the rare B decays will be measured relative to the $B^+ \rightarrow J/\psi K^+$ cross-section allowing thus the cancellation of common systematic errors. Furthermore, it can also act as a control channel for the CP violation measurement and can be used to estimate the systematic uncertainties and efficiencies of flavour tagging algorithms. Finally, the relatively large statistics for this decay allows for initial detector performance studies.

The trigger menu for the ATLAS B-physics program has been designed to take maximum advantage of the early run phases at lower luminosities ($\mathcal{L} < 10^{33}\ {\rm cm}^{-2}{\rm s}^{-1}$). Since only 5 - 10 %

of the limited bandwidth of the ATLAS trigger system is devoted to the B-physics triggers, highly efficient and selective triggers are needed. Most B-physics triggers are based on single- and di-muon events in the final state leading to a clean signature for triggers and flavour tagging [34–36]. In the early data taking period the main B-physics triggers are expected to run without a need of prescales, allowing for low $p_{\rm T}$ muon and low E_T electron triggers (the latter will be however prescaled at 10^{32} cm^{-2} s^{-1}). In general, the trigger strategy is mainly based on a single muon trigger at the first level, which could be combined with certain calorimeter trigger objects at higher trigger levels to select hadronic final states ($B_s \to D_s\pi$) or e/γ final states ($J/\psi \to e^+e^-$, $K^*\gamma$ or $\phi\gamma$). In order to not exceed the available bandwidth, in the phase of higher luminosities above $2 \cdot 10^{33}$ cm^{-2}s^{-1} the main working trigger will be based on di-muons on the first level, enabling a clean measurement of rare B-decays ($B \to \mu\mu$ or $B \to K^{*0}\mu\mu$), double semi-leptonic decays and the $B \to J/\psi(\mu\mu)$ decay channels.

3.2 Beauty production cross section determination

The $b\bar{b}$ production cross-section will be measured using inclusive and exclusive methods in parallel to control the systematics. For the inclusive methods ATLAS looks at the semi-leptonic $b \to \mu + X$ and the $B \to J/\psi(\to \mu^+\mu^-) + X$ decay modes. In the next section we will briefly describe the measurement of the exclusive $B^\pm \to J/\psi K^\pm$ cross-section. The measurement of the J/ψ mass and its detection efficiency is a central task for the analysis of the first ATLAS data, providing the tools to validate the detector by extracting muon energy scale determination in the low $p_{\rm T}$ region and detector misalignments (Sect. 3.5). Finally, the mass measurement and reconstruction efficiency for B^+, the total and differential cross-sections and its lifetime measurements will be of interest for other B-physics analyses.

The main backgrounds that are competing with the signal are single-muon from $c\bar{c}$ decays and direct J/ψ's from $pp \to J/\psi + X$. In the first case, the $p_{\rm T}$ distribution of the muons is softer as compared to the muon spectrum from $b\bar{b}$ decays while in the latter no displaced secondary vertex is expected. In consequence the following parameters are used for b-tagging:

- the signed transverse impact parameters d_0 of charged particles originating from B-meson decays at a secondary vertex due to the long lifetime of B-mesons.
- the relative transverse momentum $p_{\rm T}^{\rm rel}$ of the muon of the b-decay with respect to the axis of the associated jet.

The measurement of the $p_{\rm T}^{\rm rel}$ distribution of the selected muons offers a good possibility to determine the b-contents fraction in the offline analysis. In the rest frame of the decaying B-meson, the muon gets a high transverse momentum, which is significantly larger than in the case of charm or light quark decays. The relative transverse muon momentum, $p_{\rm T}^{\rm rel}$ can therefore be used to determine the b-content of a selected data sample by fitting Monte Carlo templates to data. For the B-mesons at ATLAS, generally decay lengths of the order of several mm are expected which are at the same order of magnitude as the expectation for D-mesons. The signed transverse impact parameter d_0 is a boost independent quantity. For large transverse momenta ($p_{\rm T}^\mu > 10$ GeV) d_0 is proportional to the lifetime of the decaying particle and positive values of d_0 are preferable. The significance of signed impact parameter for muons with an associated b-jet and the distributions of the relative transverse momentum are shown in Fig. 13 and Fig. 14 respectively. In both cases, the selection power is clearly visible.

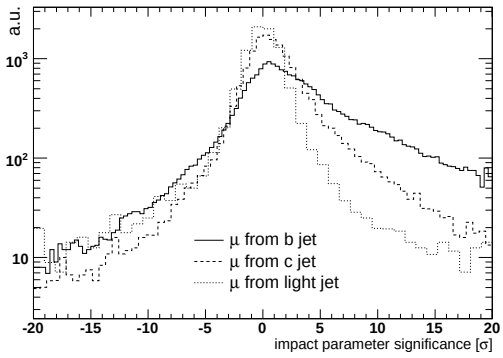

Fig. 13: The distribution of the significance of the signed impact parameter d_0/σ

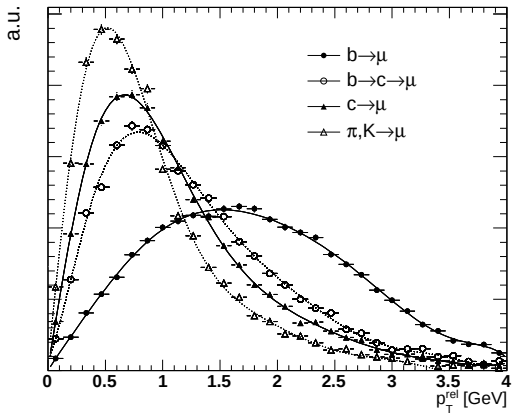

Fig. 14: The $p_{\mathrm{T}}^{\mathrm{rel}}$ distribution for different processes considered in the b-jet selection.

The $b\bar{b}$ production cross-section measurement based on the single-muon and jet requirements at the trigger level is then obtained according to the usual relation

$$\sigma(b\bar{b} \to \mu(p_{\mathrm{T}}^{\mu} > 6\ \mathrm{GeV})X) = \frac{N_b^{\mathrm{sel}}}{\int \mathcal{L}\,\mathrm{d}t} \cdot \frac{f_b}{\epsilon_b^{\mathrm{trig}} \cdot \epsilon_b^{\mathrm{rec}}} \tag{3}$$

where the b-trigger efficiency was found to be $\epsilon_b^{\mathrm{trig}} = 0.135$ and the combined muon reconstruction efficiency is $\epsilon_b^{\mathrm{rec}} = 0.85$. The determination of the b content, f_b, of the selected sample is extracted by fitting the simulated $p_{\mathrm{T}}^{\mathrm{rel}}$ distribution to the data. This can be done by a binned maximum likelihood fit taking into account the finite size of both, the data sample and the simulated Monte Carlo templates. In the signal template, the direct $b \to \mu$ and cascade $b \to c \to \mu$ contributions are contained, whereas all others are summarized in the background template. The distribution can be seen in Fig. 15. With this fit, a b-content of $f_b = 0.23$ was obtained, and a corresponding background fraction of $f_{bg} = 0.77$. The values obtained in this study are in good agreement with the values obtained by the Tevatron experiments [37]. Combining both methods, the $b\bar{b}$ production cross-section is expected to be measured with a statistical precision better than $\mathcal{O}(1\ \%)$ with $\approx 100\ \mathrm{pb}^{-1}$ of integrated luminosity. The systematic uncertainty is dominated by the luminosity measurement. It is estimated to be $10\ \%$ in the initial phase, and reduced to about $6.5\ \%$ after the first $0.3\ \mathrm{fb}^{-1}$. The scale uncertainty of the NLO calculations is about $5\ \%$, while the PDF uncertainty is estimated to be $3\ \%$. Finally, the uncertainty originating from the muon identification is about $3\ \%$, leading to a systematic uncertainty of $12\ \%$ and $9.2\ \%$ correspondingly in the initial and later phase .

3.3 B^+ reference channel

Negligible direct CP violation is expected in the $B^{\pm} \to J/\psi K^{\pm}$ decay because for $b \to c + \bar{c}s$ transitions the SM predicts that the leading and higher order diagrams are characterized by the same weak phase. The only source of asymmetry is the different interaction probability for

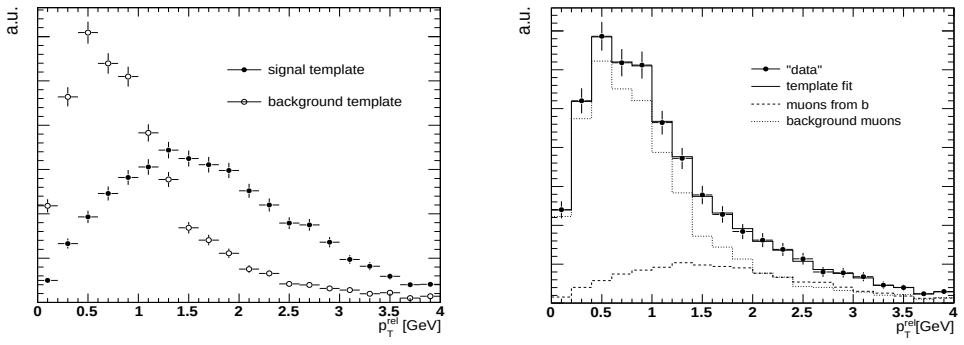

Fig. 15: The generated $p_{\mathrm{T}}^{\mathrm{rel}}$ templates (left) and fraction of the b-content of the selected b-jet sample (right) showing comparison of the fitted to the true values from Monte Carlo.

K^+ and K^- with the detector material. The B^+ candidates are reconstructed based on the $J/\psi(\rightarrow \mu^+\mu^-)$ selection, and combined with K^+ candidates formed from inner detector tracks.

The B^+ invariant mass distribution $M(K^+\mu^+\mu^-)$ of the candidates, fulfilling the selection cuts, is presented in Fig. 16 for signal and background with a maximum-likelihood fit, where the likelihood function is a Gaussian for the signal region and a linear function for the background ($b\bar{b} \rightarrow J/\psi + X$). The mass range of the fit is taken from 5.15 GeV to 5.8 GeV in order to reduce contributions from partially reconstructed B meson decays. The background at the right of the mass peak originates from misidentified π^+ from $B^+ \rightarrow J/\psi\pi^+$ decays. The fit result for the B^+ mass is: $M(B^+) = (5279.3 \pm 1.1)$ MeV with a width of $\sigma(B^+) = (42.2 \pm 1.3)$ MeV. The relative errors, scaled properly for an integrated luminosity of about 10 pb^{-1}, are about 0.02% and 3.5% respectively. The slight shoulder to the left of the mass distribution is due to the background shape in this mass region and has been included in the systematic uncertainties of the fit model.

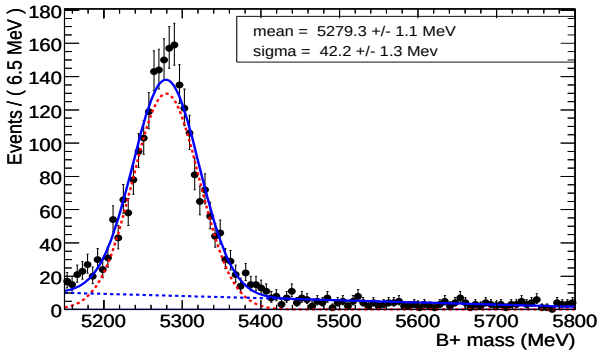

Fig. 16: B^+ mass fit with the both signal (red) and background (blue) contributions shown separately.

With the first $10\ \mathrm{pb}^{-1}$ of LHC data a total and differential production cross-section measurement of the $B^+ \to J/\psi K^+$ can be achieved. The differential cross-section $\mathrm{d}\sigma/\mathrm{d}\,p_\mathrm{T}$ can be obtained from the usual form:

$$\frac{\mathrm{d}\sigma(B^+)}{\mathrm{d}\,p_\mathrm{T}} = \frac{N_\mathrm{sig}}{\Delta p_\mathrm{T} \cdot \mathcal{L} \cdot \mathcal{A} \cdot \mathrm{BR}} \tag{4}$$

where N_sig is the number of reconstructed B^+ obtained from the mass fit and the size of the p_T bin is denoted with Δp_T. Furthermore, $\mathcal{L}$ is the total luminosity to which the dataset corresponds and is obtained from PYTHIA output and BR is the product of the branching ratios using the world average [38] branching ratios of $\mathrm{BR}(B^+ \to J/\psi K^+) = (10.0 \pm 1.0) \times 10^{-4}$ and $\mathrm{BR}(J/\psi \to \mu^+\mu^-) = (5.88 \pm 0.10) \times 10^{-2}$. The overall efficiency $\mathcal{A}$ is calculated for each p_T range separately as the ratio of the number of signal events determined from the previous fit procedure and the number of the Monte Carlo signal events within the same p_T range. To measure the B^+ total cross-section a similar procedure with that used for the calculation of the differential cross-section is followed.

The measurement of the lifetime τ of the selected B^+ candidates is a sensitive tool to confirm the beauty content in a sample, in particular the number of the reconstructed $B^+ \to J/\psi K^+$ decays obtained in the $b\bar{b} \to J/\psi X$ dataset. The proper decay-time is defined as $t = \lambda/c$. The proper decay-time distribution in the signal region $B^+ \to J/\psi K^+$ can be parametrized as a convolution of an exponential function with a Gaussian resolution function, while the background distribution parametrization consists of two different exponential functions, where each is convoluted with a Gaussian resolution function. In the $b\bar{b} \to J/\psi X$ no zero lifetime events are expected since there is no prompt J/ψ produced. In the realistic case, where zero lifetime events will be present, an extra Gaussian centered at zero is needed in order to properly describe those events.

The results on the lifetime measurements are shown in Fig. 17. The background can be best described with the two lifetime components (τ_1 and τ_2). For the events in the mass region of the signal within $M(B^+) \in [5.15, 5.8]\ \mathrm{GeV}$ the proper decay-time found from the decay length is compared to the generated B^+ lifetime. The differences are well centered at zero with a Gaussian distribution and sigma $0.088\ \mathrm{ps}$. It should be noted that the resolution as well as its σ in η bins of 0.25 is found to be independent of η.

3.4 Open flavour: rare B-decays

Flavour changing neutral currents, a direct transition from $b \to d/s$, are forbidden at the tree level in the SM and occur at the lowest order through one loop diagrams. They are a sensitive test of the SM and its possible extension(s), providing information on the long distance QCD effects and enabling a determination of the CKM matrix elements $|V_{td}|$ and $|V_{ts}|$. Furthermore, some of the rare decay channels contribute to the background for other channels, which are very sensitive to BSM effects.

An upper limit of the branching ratio $BR(B_s^0 \to \mu^+\mu^-) = (1-2) \cdot 10^{-8}$ at $90\ \%$ confidence level or of $(2-3) \cdot 10^{-8}$ at 3σ evidence based on $N_B = 1.1$ events that can already be extracted from an integrated luminosity of $2\ \mathrm{fb}^{-1}$. This is clearly better than the current CDF limit of $4.7 \cdot 10^{-8}$ at $90\ \%$ confidence level. Already at $1\ \mathrm{fb}^{-1}$ ATLAS is able to collect $\mathcal{O}(10^6)$

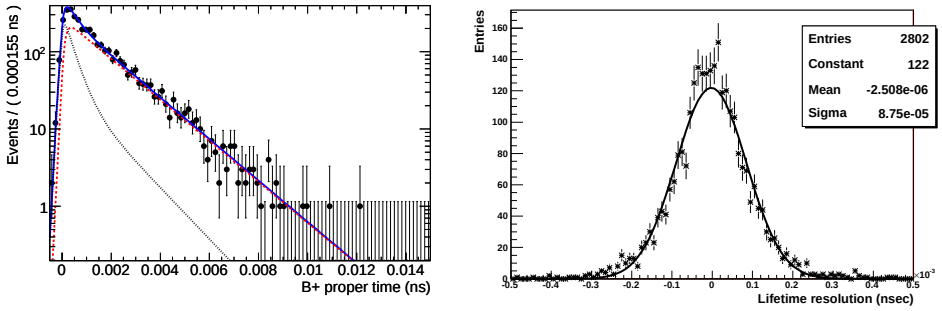

Fig. 17: The B^+ lifetime fit (left) with the signal (dashed red) and the background (dashed black) contributions shown separately. The B^+ lifetime resolution (right).

di-muon events in the mass window of $4\ \mathrm{GeV} < M(\mu^+\mu^-) < 7\ \mathrm{GeV}$. This is after the selection based on cuts on p_{T}, the invariant mass $M_{\mu^+\mu^-}$, the transverse decay length L_{xy} of the di-muon system, and on isolation requirements. Based on this data, an upper limit on the number of signal events, N_B, corresponding to a given confidence level will be determined. The main background sources originate from combinatorial decays as $b\bar{b} \to \mu^+\mu^- X$, from misidentifications ($B_s^0 \to \pi^+\pi^-$, $B_s^0 \to K^+K^-$, $B_s^0 \to \pi^+K^-\nu_\mu$) or from other rare decays ($B_s^0 \to \mu^+\mu^-\mu^+\nu_\mu$, $B_s^0 \to \mu^+\mu^-\gamma$). N_B will be used to extract the upper limit on the $B_s^0 \to \mu^+\mu^-$ branching ratio $BR(B_s^0 \to \mu^+\mu^-)$, using the reference channel $B^+ \to J/\psi K^+$ as described in Sec. 3.3, since trigger and offline reconstruction efficiencies largely cancel for di-muons in these channels. In this procedure, a ratio of geometric and kinematical acceptances of the signal and the reference channel will be determined from the Monte Carlo simulations. With an integrated luminosity of $30\ \mathrm{fb}^{-1}$, corresponding to three years of initial data taking, the SM predictions could be tested with a $3\ \sigma$ sensitivity. The continuation of this measurement at nominal LHC luminosities has been proved to lead to a clear statement with a $5\ \sigma$ sensitivity after already one additional year of data taking at design luminosity of $10^{34}\mathrm{cm}^{-2}\mathrm{s}^{-1}$.

3.5 Quarkonia

Understanding the production of prompt quarkonia at the LHC is an important step to understand the underlying QCD mechanisms, and one that has given rise to controversy, both with respect to the cross-section magnitude [39] and the polarization [40]. The initial discrepancy in cross-section led to the Color Octet Model [41] but more high p_{T} results are needed to distinguish between this and competing models.

In addition to these open questions, the narrow J/ψ and Υ resonances are ideal for studies of detector performance. The expected abundant production (see Fig. 18) makes this feasible already in the very early data. Both decay channels $J/\psi\ (\Upsilon) \to \mu^+\mu^-$ and $J/\psi\ (\Upsilon) \to e^+e^-$ will be used as tools to test our detector performance. In the following we consider only the J/ψ and $\Upsilon(1S)$ resonances. Quarkonia selection in ATLAS is mainly based on a di-muon trigger which requires two identified muons, both with $p_{\mathrm{T}} \geq 4\ \mathrm{GeV}$ and within a pseudorapidity of

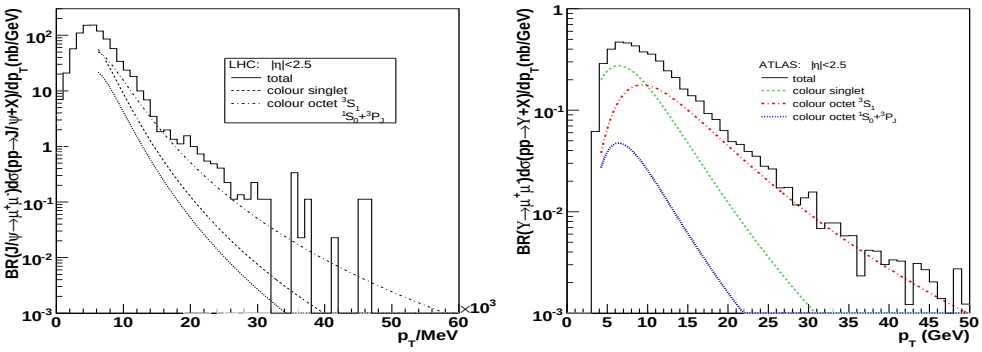

Fig. 18: Differential J/ψ and Υ cross-sections as predicted from the Color Octet Model. Contributions from (singlet) χ production is included.

$|\eta| < 2.4$. The di-muon sample considered here has offline p_{T} cuts of 6 and 4 GeV applied to the two identified muons. To suppress backgrounds (decays-in-flight, heavy flavour decays) we require tracks to come from the same vertex and with a pseudo-proper time cut of $\tau = 0.2$ ps, defined as $\tau = \frac{M \cdot L_{xy}}{p_{\mathrm{T}}(J/\psi) \cdot c}$. In Fig. 19 (left) the resulting di-muon spectrum with background contributions is shown. We expect 15000 J/ψ's and 2500 $\Upsilon(1S)$ per pb^{-1}. The mass resolution for $J/\psi \to \mu^+\mu^-$ is expected to be 53 MeV, and for $\Upsilon \to \mu^+\mu^-$ we found 161 MeV on average.

We are also studying the possibility of doing performance measurements using di-electron resonances. In that case the E_{T} cut for both leptons is 5 GeV at trigger level and offline, and $|\eta| < 2$. Tight electron identification cuts are applied to reject background, including E/p, vertexing layer hit on the tracks, and the ratio of high to low threshold hits in the transition radiation tracker. We expect 2500 J/ψ's and 500 $\Upsilon \to e^+e^-$ per pb^{-1} with an instantaneous luminosity of 10^{31} cm^{-2} s^{-1}. The mass resolution for $J/\psi \to e^+e^-$ is expected to be about 200 MeV, see Fig. 19 right. The width is mainly constrained by bremsstrahlung due to the large amount of material in the inner detector.

In addition to cross-section measurements ATLAS will use the quarkonia di-muon decays to provide answers to the polarization puzzle and help constrain the models. Defining the polarization parameter α as $\alpha = (\sigma_T - 2\sigma_L)/(\sigma_T + 2\sigma_L)$, we can measure this by θ^*, the angle between J/ψ in rest frame and μ^+, as they are related by:

$$\frac{dN}{d\cos\theta^*} = C \cdot \frac{3}{2\alpha + 6} \cdot (1 + \alpha \cos^2\theta^*) \tag{5}$$

With the di-muon triggers we get a rather narrow $\cos\theta^*$ distribution, with both muons having similar p_{T}. To access higher values of $\cos\theta^*$ we utilize a single muon trigger where we can pair the trigger muon with a low p_{T} track to get large Δp_{T} and $\cos\theta^*$ (see Fig. 20 left). For the result quoted here we used a trigger threshold of 10 GeV for the single muon trigger and the p_{T} requirement on the second track was 0.5 GeV. The looser cuts allow for more background but still with decent signal to background discrimination ($S/B = 1.2$ for J/ψ). This dataset was added (with corrections for overlaps) to complement the di-muon triggered dataset. The

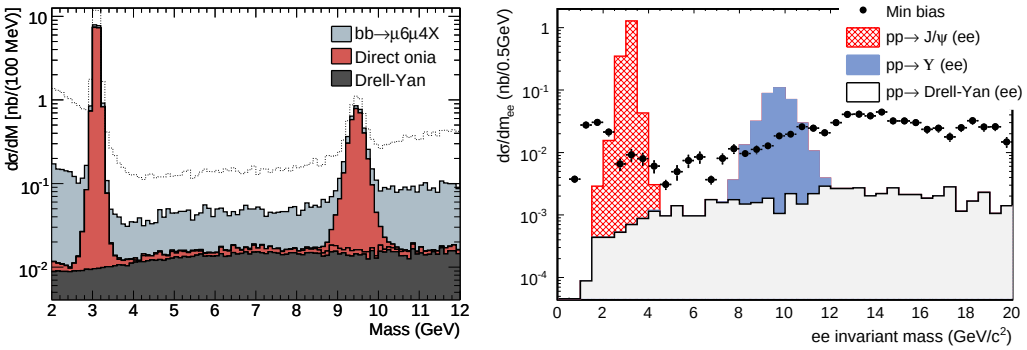

Fig. 19: Di-electron mass distributions for muons (left) and electrons (right). In the left plot the spectrum in case of no vertex cuts (top dashed line) is also shown.

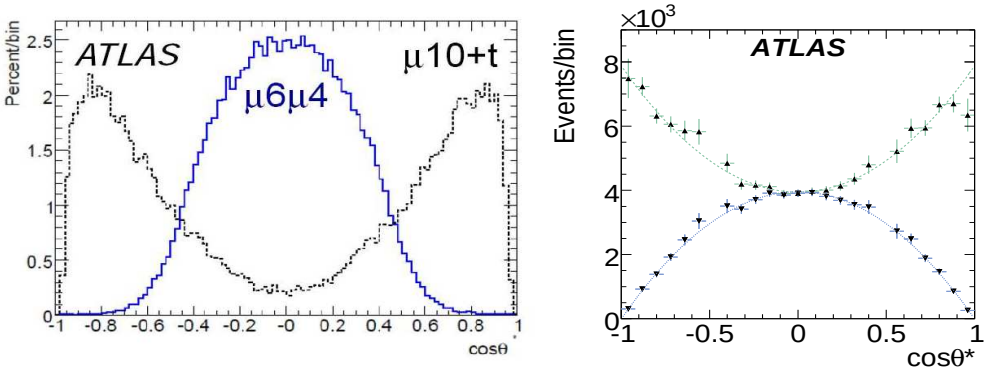

Fig. 20: Left: $\cos\theta^*$ distributions for double and single muon triggered events. Right: Fit to combined events in $p_{\mathrm{T}} \in [12, 13]$ GeV. Top shows longitudinally polarized ($\alpha = -1$) and bottom transverse polarized ($\alpha = 1$) events.

combined $\cos\theta^*$ distributions were then fitted for α and C in slices of p_{T}. With unpolarized samples the results are given in Table 2 for 10 pb^{-1}. Similar tests have been carried out with $\alpha = \pm 1$. An example is shown in Fig. 20 right.

We expect to be able to measure the J/ψ polarization with the p_{T} of the J/ψ in the range of 10 GeV (trigger dependent) up to 50 GeV. Already with the first 10 pb^{-1} we can achieve better precision than the current Tevatron measurements - but with J/ψ at high p_{T}, which is what is needed to truly distinguish between models. For $\Upsilon(1S)$ we can get the same precision with 100 pb^{-1}. In this latter case we have acceptance all the way down to $p_{\mathrm{T}} \approx 0$ for the Υ, which will be a very useful region to compare with the Tevatron results.

Table 2: 10 pb^{-1}: Measured values of α in p_{T} bins in simulated datasets with $\alpha = 0$.

p_{T} (GeV/c)	9 - 12	12 - 13	13 - 15	15 - 17	17 - 21	> 21
$\alpha(J/\psi)$	0.156 $\pm$0.166	-0.006 $\pm$0.032	0.004 $\pm$0.029	-0.003 $\pm$0.037	-0.039 $\pm$0.038	0.019 $\pm$0.057
$\alpha(\Upsilon)$	-0.42 $\pm$0.17	-0.38 $\pm$0.22	-0.200 $\pm$0.20	0.08 $\pm$0.33	-0.15 $\pm$0.18	0.47 $\pm$0.22

3.6 Conclusions

The ATLAS experiment has a rich B-physics program [42] based on clearly defined trigger strategies for all luminosity phases of the LHC. These measurements will contribute to CP violation studies with B_s-mesons and its sensitivity to BSM as well in studies of rare B decays and quarkonia production. The precision measurement of B-physics processes are an alternative method to explore the presence of new physics at LHC in addition to the direct SUSY searches.

Two inclusive methods for beauty cross-section measurements to be used mainly at the early data taking period of ATLAS were presented. The first method is using the J/ψ signature with detached vertices, while the second one is based on semileptonic $b \to \mu$ decays. The two methods are complementary and the plan is to apply them simultaneously since both signatures will be available with early data. The two methods rely on different trigger algorithms and different physics processes and signatures, therefore the cross-section results obtained from each one can be used for cross checking calibrations of the trigger algorithms used in the measurements. Combining these two methods, the $b\bar{b}$ production cross-sections measurement is expected to reach a statistical precision of $\mathcal{O}(1\ \%)$ after one month of data taking, if the initial LHC luminosity will be $\mathcal{L} = 10^{31}\ \mathrm{cm}^2\mathrm{s}^{-1}$, whereas a systematic uncertainty of $\mathcal{O}(12\ \%)$ is expected. Furthermore, the reference channel $B^+ \to J/\psi K^+$ has been studied and it could be shown, that a lifetime measurement is a good tool to confirm the b content of the selected sample.

In the first data taking period ATLAS will also measure the J/ψ and Υ cross-sections, taking advantage of the favorable trigger situation in the early data. A method to determine the level of polarization is also presented. We expect to measure the J/ψ polarization to within 0.02 - 0.06 in the first 10 pb^{-1}, dependent on the polarization itself.

4 Heavy flavour production in the CMS experiment at the LHC

Authors: M. Biasini and A. Starodumov

4.1 Introduction

There are several reasons why a general purpose detector like CMS designed for high p_{T} physics could be efficiently used to study heavy flavour physics. First of all, there will be about 10^{11} $b\bar{b}$ pairs produced at the initial luminosity year of $10^{32}\ \mathrm{cm}^{-2}\mathrm{s}^{-1}$ thanks to the high $b\bar{b}$ x-section which is $\sigma_{b\bar{b}} \sim 500\,\mu b$ at $\sqrt{s} = 14\,\mathrm{TeV}$. So, very rare decays like $B_s^0 \to \mu^+\mu^-$and $B_s^0 \to \gamma\mu^+\mu^-$ could be searched even with the Standard Model (SM) decay rate. In different scenarios

of New Physics (NP) the branching fraction of these decays could be enhanced by orders of magnitude, which makes the observation of these channels even more probable.

From the detector point of view heavy flavour physics is also an attractive field. Thanks to the low p_{T} (di)-muon triggers, precise vertex detector and efficient tracker system, the CMS detector is capable of efficiently recognizing and reconstructing specific topologies of b-decays. On the other hand, the study of b-jets provides with an important knowledge which might be crucial in searches for Higgs boson and supersymmetric particles. Also, one should not forget that b- and heavy onia-decay channels provide an excellent calibration opportunity for the vertex and tracker systems.

And finally, at the low luminosity phase there are no expectations to observe Higgs decays, but as it is mentioned above there are plenty of $b\overline{b}$. So, first real physics results at LHC could be obtained in the heavy flavour sector. Even at a high luminosity, thanks to efficient (di)-muon trigger, CMS is able to continue such studies.

4.2 The CMS detector

The complete description of the CMS detector can be found elsewhere [43]. Here only the main characteristics are mentioned. The CMS detector is a standard general purpose hadron collider detector composed of the following subsystems: vertex and tracker systems, electro-magnetic and hadron calorimeters and muon system. The full length is 22 m and outer diameter is 15 m. The total weight of the detector is $12.5\,\mathrm{kton}$. All subsystems but the muon detector are placed inside a superconducting magnetic coil which is able to reach a $3.8\,\mathrm{T}$-field. In the following, the most crucial subsystems for heavy flavour physics are briefly discussed.

4.2.1 Muon system

The CMS muon system is composed of three types of gaseous particle detectors for muon identification. Drift tubes (DT) chambers in a central barrel region and cathode strip chambers (CSC) in two end-cap regions, thanks to a high spatial resolution, are used for position and momentum measurements. Because of their fast response time, both systems are also provide the Level-1 trigger with good efficiency and high background rejection. Resistive plate chambers (RPC), which are placed in both the barrel and end-cap regions, combine an adequate spatial resolution with an excellent (≤ 5 ns) time resolution. Along with the DT and CSC systems, the RPC system provides the Level-1 trigger. It also capable to identify unambiguously the relevant bunch-crossing to which a muon track is associated even in the presence of the high rate and background at a full LHC luminosity.

Muon identification efficiency in the central region ($|\eta| < 1$) is above 70% for muons with $p_{\mathrm{T}} > 5$ GeV/c. In the endcap regions ($1 < |\eta| < 2.5$) identification efficiency is above 70% already for muons with $p_{\mathrm{T}} > 3$ GeV/c.

4.2.2 Tracker system

The CMS tracker system based only on silicon detectors (220 m^2 of Si): micro-strip and pixel. The strip detector consists of 10 barrel layers and 9 disks positioned both forward and backward. Depending on rapidity the high p_{T} tracks leaves 10 to 14 hits. The hit resolution is ~ 50 μm in

$r-\phi$ direction and ~ 500 μm in z-direction. The pixel system is placed closer to the interaction point and consists of 3 barrel layers and 2 disks positioned both forward and backward. Since pixel dimension is 100×150 μm^2 the detector provides precise 2D information. The hit resolution is ~ 10 μm in $r-\phi$ direction and ~ 17 μm in z-direction. Momentum resolution of the CMS tracker system varies from 0.5 % in the central region to 2 % in the endcaps for tracks with $p_{\mathrm{T}} = 1 \div 10$ GeV/c. The primary and secondary vertex resolution is event dependent. Ussually, for b-decay channels the primary vertex resolution in the transverse plane is about 20 μm and the secondary one is $70 \div 100$ μm.

4.3 Trigger strategies

Triggering in CMS is done in two steps. The Level-1 trigger is based on muon and calorimetry information. It has a latency of $3.2\,\mu$s with a goal to reduce an event rate from 40 MHz to 100 kHz. At the second step called High-Level Trigger (HLT), information from all subsystems are readout and used in the event reconstruction. The reconstruction should be fast, therefore it is done locally: topologically around Level-1 pattern. At HLT the event rate decreases from $100\,$kHz to $100\,$Hz.

B-physics events are relatively soft. Hence, Level-1 calorimetry triggers having high E_{T} thresholds do not 'see' such events. Only events with one or two muons in the final state can be triggered with high selection efficiency for soft $b\overline{b}$ events (see, for example, the Level-1 trigger menu in [44]). The transverse momentum thresholds of these triggers depend on an instantaneous luminosity, but will be kept as low as possible in the range $p_{\mathrm{T}} > 7 \div 14$ GeV/c for single and $p_{\mathrm{T}} > 3 \div 7$ GeV/c for di-muon triggers. At HLT, exclusive and inclusive b-triggers, based on partial reconstruction of searched b-decay channels, are used. For the final states with two muons, a selection procedure which is used the reconstructed di-muon secondary vertex significantly improves a signal over background ratio. The detailed description of the trigger algorithms can be found in [45].

4.4 Physics channels

The CMS heavy flavour menu could be subdivided into two categories. The first one is approved results, which will be reported further. The second category is not finished or not yet approved by the Collaboration active studies. The last category will be only mentioned below.

4.4.1 Inclusive b production

Three different mechanisms contribute to the heavy flavour production at hadron colliders: gluon splitting, gluon/quark fusion and flavour excitation. Each of these production mechanism has its own final state topology. It is important to measure the B-hadron p_{T} spectra within a large range to be able to disentangle the contributions of those mechanisms. In CMS the measurement of the inclusive b production cross section will be done with events containing jets and at least one muon.

The measurement of the differential cross sections is studied for B-hadrons of $p_{\mathrm{T}} > 50$ GeV/c and within the rapidity region of $|\eta| < 2.4$. The event selection requires a b-tagged jet to be present in the event. B tagging is based on inclusive secondary vertex reconstruction in

jets [46]. As the Level-1 trigger, the single muon one is used with the threshold of 19 GeV/c. At HLT in addition to the muon a b-jet with $p_{\mathrm{T}} > 50$ GeV/c is required.

The signal fraction is determined from a fit to the data distribution using the simulated shapes for the signal and background. Each reconstructed muon is associated to the most energetic b-tagged jet. The average efficiency of associating the muon with the b-tagged jet is 75%. The transverse momentum of the muon with respect to the b-jet axis discriminates signal against background.

Several sources of systematic uncertainties are considered in the study [47]. The largest uncertainty arises from the 3% error on a jet energy scale which leads to a cross section error of 12% at $p_{\mathrm{T}} > 50$ GeV/c.

1.6 million b-events for 1 fb^{-1} of an integrated luminosity will be collected to investigate the b production mechanism in CMS. The b purity of the selected events varies as function of the transverse momentum in a range from 70% to 55%. The b production cross-section at $p_{\mathrm{T}} = 1.2$ TeV/c can be measured with 20% uncertainty.

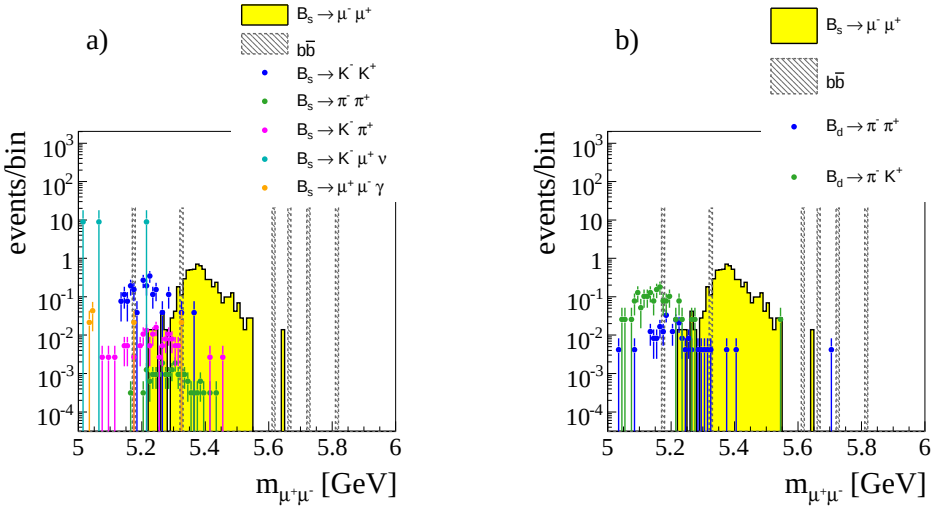

Fig. 21: Background $m_{\mu\mu}$ distribution after the application of all selection criteria (with factorizing selection criteria) for all channels that are left: a) B_s decays, b) B_d decays.

4.4.2 $B_s^0 \to \mu^+\mu^-$

Purely leptonic B-decays are theoretically very clean, thus providing an ideal environment for seeking indirect hints of NP effects. The SM branching ratio of $B_s^0 \to \mu^+\mu^-$ is very small, $(3.42 \pm 0.54) \cdot 10^{-9}$ [48], while in large-$\tan\beta$ NP models it can be enhanced by orders of magnitude [49]. Up to now only the upper limit on the branching ratio is set by the CDF Collaboration: 4.7×10^{-8} at the 90% C.L. [50].

The main challenge in the measurement of the $B_s^0 \to \mu^+\mu^-$ decay rate is background suppression. Many background sources can mimic the signal topology. First, non-resonant $b\bar{b}$ events

Table 3: Background for $B_s^0 \to \mu^+\mu^-$ samples used in the analysis. The visible cross-section, and the corresponding number of events for 10 fb^{-1} is given. The visible cross-sections include fragmentation, branching fractions, and (fake) muon $p_{\rm T}$ and $|\eta|$ selection criteria. The numbers $N_{\mu ID}$ do not yet include any selection criteria but hadron misidentification probability.

Sample	Generator cuts/channels	σ_{vis}[fb]	$N_{\mu ID}$ (10 fb^{-1})
$b\bar{b} \to \mu^+\mu^- + X$	$p_{\rm T}^{\mu} > 3\,{\rm GeV}/c$, $\lvert\eta^{\mu}\rvert < 2.4$ $p_{\rm T}^{\mu\mu} > 5\,{\rm GeV}/c$ $0.3 < \Delta R(\mu\mu) < 1.8$ $5 < m_{\mu\mu} < 6\,{\rm GeV}/c^2$	1.74×10^7	1.74×10^8
B_s decays	$B_s \to K^-K^+$	2.74×10^5	274
	$B_s \to \pi^-\pi^+$	9.45×10^3	3
	$B_s \to K^-\pi^+$	3.08×10^4	16
	$B_s \to K^-\mu^+\nu$	2.80×10^5	2.80×10^4
	$B_s \to \mu^+\mu^-\gamma$	1.29×10^1	130
B_d decays	$B_d \to \pi^-\pi^+$	8.34×10^4	21
	$B_d \to \pi^-K^+$	3.74×10^5	187
	$B_d \to \pi^-\mu^+\nu$	1.25×10^6	6.25×10^4
	$B_d \to \mu^+\mu^-\pi_0$	3.77×10^1	377
B_u decay	$B_u \to \mu^+\mu^-\mu^+\nu$	2.24×10^3	2.24×10^4
B_c decays	$B_c \to \mu^+\mu^-\mu^+\nu$	2.01×10^1	201
	$B_c \to J/\psi\mu^+\nu$	1.89×10^3	1.89×10^4
Λ_b decays	$\Lambda_b \to p\pi^-$	4.22×10^3	1
	$\Lambda_b \to pK^-$	8.45×10^3	1
QCD hadrons	$5 < M(hh) < 6\,{\rm GeV}/c^2$	2.24×10^{11}	1.12×10^8

with each $b \to \mu X$ decays. Second, non-resonant QCD events, where two high $p_{\rm T}$ hadrons are misidentified as muons. And finally, rare B_d, B^+, B_s and Λ_b decays, comprising hadronic, semileptonic, and radiative decays. Some of these decays constitute a resonant background, like $B_s \to K^+K^-$, others have a continuum di-muon invariant mass distribution. Potentially, the resonant background is the most dangerous one. But the contribution from such backgrounds is negligible due to the excellent mass resolution provided by the CMS detector. Fig. 21 shows background $m_{\mu\mu}$ distribution after the application of all selection criteria for all channels that are left.

The current background simulation does not include muon samples due to hadronic in-flight decays or punch-through. It has been estimated that this hadronic component will increase the background level by about 10% (see Fig. 5.10.9 in [51]). Table 3 summarizes studied so far background samples. The probabilities for hadron misidentification used to calculate expected number of background events in CMS are found to be $\varepsilon_\pi = 0.5\%$, $\varepsilon_K = 1.0\%$, $\varepsilon_p = 0.1\%$.

As the Level-1 trigger the di-muon one with a threshold of $p_{\rm T} > 3$ GeV/c for each muon is used. The HLT strategy relies critically on the tracker detector for a fast and high-efficiency reconstruction of the primary and secondary vertexes, the determination of muon momenta and the mass of the muon pair. Two muons are reconstructed with only 6 hits per a track in the tracker system and required to have transverse momentum of $p_{\rm T} > 4$ GeV/c, to be in the central part of the detector $|\eta| < 2.4$ and to have opposite charges. Vertexing the two muons provides a powerful handle in the rate reduction: the quality of the vertex fit must be $\chi^2 < 20$. The three-dimensional flight length is required to be $l_{3D} > 150\,\mu$m. The invariant mass of the muon pair is required to be in a tight window (150 MeV/c^2) around the B_s meson mass.

For the offline analysis all tracks are reconstructed with full detector information. The same as above but tighter (e.g. $\chi^2 < 1$) and additional selections are used to suppress background. The $\eta\phi$ separation of the two muons $\Delta R(\mu\mu) = \sqrt{\Delta\eta^2 + \Delta\phi^2}$ a powerful discriminator against gluon-gluon fusion background with both b-hadrons decaying semileptonically and must be in the range $0.3 \div 1.2$. The transverse momentum vector of the B_s candidate must be close to the displacement of the secondary vertex from the primary vertex: the cosine of the opening angle between the two vectors must fulfill $\cos(\alpha) > 0.9985$. The isolation I is determined from the B_s candidate transverse momentum and charged tracks with $p_{\rm T} > 0.9$ GeV/c in a cone with half-opening $r = 1.0$ around the di-muon direction as follows: $I = p_{\rm T}^{\mu\mu}/(p_{\rm T}^{\mu\mu} + \sum_{trk} |p_{\rm T}|)$ and required to be $I > 0.85$. The significance of the flight length is required to be $l_{3D}/\sigma_{3D} > 18.0$. Mass separation between a di-muon candidate and the nominal B_s mass should not exceed 100 MeV/c^2.

For an integrated luminosity of 10 fb^{-1}, the expected number of signal events is $n_S = 6.1 \pm 0.6_{stat} \pm 1.5_{sys}$. The number of background events is $n_B = (14.1)^{+22.3}_{-14.1}$. An upper limit, extracted using the Bayesian approach, is $Br(B_s^0 \to \mu^+\mu^-) < 1.4 \cdot 10^{-8}$ at the 90% CL [52].

4.4.3 $B_s \to J/\psi\phi$

Important properties of B_s^0 system can be studied with the decay channel $B_s^0 \to J/\psi\phi$, such as the width and mass difference of the two weak eigenstates: $\Delta\Gamma_s, \Delta m_s$. In addition, the decay $B_s^0 \to J/\psi\phi$ is a golden channel for CP violation measurements. The particular spin structure of this decay allows to express its time dependence in a particular basis, called *transversity basis*, as the sum of 6 amplitudes where physical parameters enter differently. The most important of them is the weak phase ϕ_s which is at present strongly constrained by CKM fits [53] and could represent a clear hint of NP if found to be significantly different from this prediction. At present the flavour tagging tools required to extract the weak phase are not yet available in CMS and only the mixing measurement is considered here.

The Level-1 trigger is based on di-muon selection with $p_{\rm T} > 3$ GeV/c each. HLT is the same as the one for $B_s^0 \to \mu^+\mu^-$, with additional requirement for the di-muon invariant mass to be within 150 MeV/c^2 of the J/ψ mass. The J/ψ vertex is required to be 3σ away from the primary vertex. The cosine of the angle between the transverse momentum vector and the transverse decay length vector of the J/ψ candidate is required to exceed 0.9. ϕ candidates are reconstructed from all oppositely charged track pairs and all pairs with invariant mass within 20 MeV/c^2 of the ϕ mass are retained. All four tracks are then used for B_s^0 candidates, requiring invariant mass within 200 MeV/c^2 of nominal one. The transverse momentum of ϕ and B_s^0

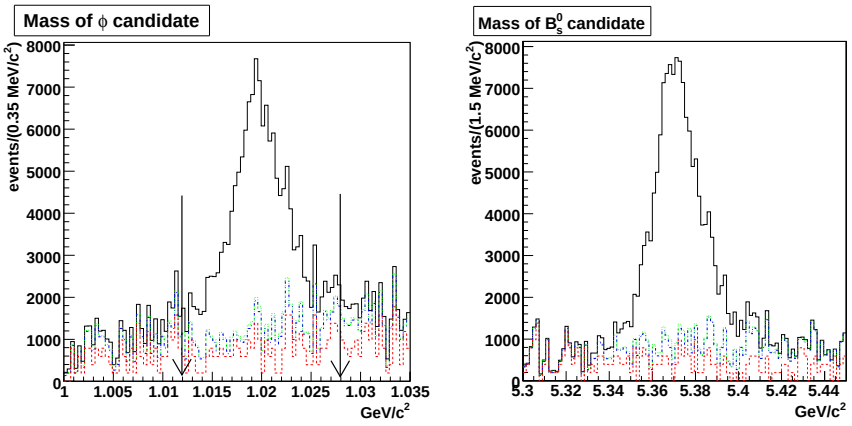

Fig. 22: Invariant mass of ϕ (left) and B_s (right) candidates after all other cuts (except for the ϕ mass requirement) have been applied; the selection on the ϕ mass is indicated. Background is from inclusive $b \to J/\psi X$ (red dashed line), from $B_d^0 \to J/\psi K^{*0}$ (blue dashed-dotted line), and from combinatorial in signal events (green dotted line).

candidates are required to be greater than 1.0 and 5.0 GeV/c, respectively.

The offline analysis follows the same criteria of HLT, but with complete information and tighter cuts. The main backgrounds arise from prompt J/ψ and $B_d^0 \to J/\psi K^{*0}$ events. Fig. 22 shows invariant mass of ϕ and B_s candidate distributions after all but ϕ mass selections applied. From an untagged time-dependent analysis of B_s^0 candidates the mixing parameters can be extracted. The result of the analysis shows that a first measurement of $\Delta\Gamma_s/\Gamma_s$ can be made with 20% precision with an integrated luminosity of 1.3 fb^{-1}, while 5% precision can be reached with 10 fb^{-1} [54].

4.4.4 $B_c^{\pm} \to J/\psi\pi^{\pm}$

The interest to the B_c meson relates to the uniqueness of the heavy-heavy quark system which carries flavour. The B_c meson has been observed at Tevatron and its mass and lifetime have been measured [55]. But available statistics does not allow to make such measurements precise enough and investigate properties of this system in details.

In CMS a feasibility study has been performed in the decay channel $B_c^{\pm} \to J/\psi\pi^{\pm}$ [56]. First J/ψ candidates are composed by two muons with $p_{\rm T} > 4$ GeV/c and $|\eta| < 2.2$ with opposite charge. The candidate invariant mass is required to be in the region from 3.0 to 3.2 GeV/c^2. Then, pion candidates are selected by requiring a third track coming from the same vertex as the two muons with $p_{\rm T} > 2$ GeV/c and $|\eta| < 2.4$. The following selections are applied in addition: a proper decay length $L_{xy}^{PDL} > 60$ μm, a significance $L_{xy}/\sigma_{xy} > 2.5$ and a opening angle between the vector from primary to secondary vertex and the momentum vector of the reconstructed B_c : $cos\theta > 0.8$.

For 1 fb^{-1} 120 signal and less than 3 background events are expected. The reconstructed B_c mass is 6.4 GeV/c^2 and the width of the mass peak is 15 MeV/c^2. To extract the B_c meson

lifetime a binned likelihood fit was performed, resulting in $\tau = 460 \pm 45$ fs.

4.4.5 Additional heavy flavour decays

Although the following analysis are not yet finalized, it is worth while to list them here to demonstrate a future spectrum of heavy flavour activity in CMS.

Measurements of $b\overline{b}$ production cross-section and lifetimes of B-mesons will be done in the following decay channels: $B^{\pm} \rightarrow J/\psi K^{\pm} \rightarrow \mu^{+}\mu^{-}K^{\pm}$, $B \rightarrow D^{0}\mu X$, $b \rightarrow J/\psi + X \rightarrow \mu^{+}\mu^{-} + X$. The correlation study of J/ψ vs μ provides clean measurements of $b\overline{b}$ production mechanisms. Searches for NP is also planned to be done in $B_s \rightarrow \mu^{+}\mu^{-}\gamma$, $B \rightarrow (\phi, K^{*}, K_s)\mu^{+}\mu^{-}$ decay channels.

4.5 Conclusions

While designed for high-p_{T} physics, the CMS has a broad heavy flavour program. Main features which allow this program are 1) high $b\overline{b}$ event rate even at a low ($10^{32} - 10^{33}$) initial luminosity, 2) the efficient low p_{T} di-muon trigger and 3) excellent tracking that provides high momentum, mass, vertex resolution. Expected results are competitive with current B-physics experiments.

Acknowledgments
One of us (A.S.) would like to thank V. Ovakimian for his help in the preparation of this paper.

5 Top production in the CMS experiment at the LHC

Authors: C. Rosemann and R. Wolf

5.1 Top quark pair production in CMS

The LHC will provide proton proton collisions at center-of-mass energies of $14\,(10)\,\mathrm{TeV}$ with a specific luminosity of $\approx 10\,(0.1)\,\mathrm{nb}^{-1}\mathrm{s}^{-1}$. This will allow the inclusive production of top anti-top quark pairs at a rate of 100-$(10)\,\mathrm{Hz}$ (where the values in parenthesis are given for startup). The cross section for the production of top anti-top quark pairs in proton proton collisions at these center-of-mass energies is expected to be $908 \pm 83 \pm 30\,\mathrm{pb}$ ($414 \pm 40 \pm 20\,\mathrm{pb}$)) [57], where the first error reflects scale uncertainties and the second error uncertainties in the choice and parametrization of parton density functions (PDFs). In the standard model (SM) top anti-top quark pair production is dominated by gluon gluon fusion (with a fraction of $\approx 90\%$). As top quark production at the reached center-of-mass energies and luminosities at HERA is unaccessible the obvious impact of the HERA experiments on top production at the LHC lies in the determination of the most undefined gluon density function and thus in the reduction of the second uncertainty of the above cross section estimate. In figure 23 (left) three sets of different PDFs from the two HERA experiments H1 and ZEUS and from the CTEQ collaboration are shown at a scale of $Q^2 = 10\,\mathrm{GeV}^2$. Due to kinematics and reconstruction requirements these PDFs will mostly be probed at large scales and medium to high proton momentum fraction $x > 0.01$, where these PDFs show smallest uncertainties and deviations.

In the beginning the emphazise will be put on the rediscovery of the top quark within the first $(50\text{-}100)\,\mathrm{pb}^{-1}$, followed by inclusive cross section measurements based on robust selection

methods and first attempts to determine the top mass and differential cross sections with target luminosities of $\approx 1\,\mathrm{fb}^{-1}$. An important aspect of top quark physics will be the capacity of top anti-top quark pair production of being a standard candle witin the SM to exploit and demonstrate the detector understanding of the two major experiments ATLAS and CMS. The rediscovery of the top quark in early data taken with the CMS detector and prospects for first mass measurements in $\approx 1\,\mathrm{fb}^{-1}$ will be discussed in the following.

5.2 Rediscovery of the top quark

As an example for the rediscovery potential of the top quark within the first data a recent study in the semi-leptonic decay channel with a muon in the final state is presented [58]. It was performed for a target luminosity of $10\,\mathrm{pb}^{-1}$ of data at a center-of-mass energy of $14\,\mathrm{TeV}$ taken with the CMS detector. The conclusions may though be translated into equivalent conclusions for a luminosity of $50\,\mathrm{pb}^{-1}$ of data at a center-of-mass energy of $10\,\mathrm{TeV}$. Focus was put on robust and simple selection methods with minimal dependency on detector components that may be least understood during startup. Main backgrounds are considered to be W or Z boson production with additional hard jets and QCD mulitjet production with leptons from b/c quark or in-flight decays which are mis-interpreted as originating from real W decays. Inclusive top anti-top pair production and W and Z boson production were produced with the Alpgen event generator for $2 \rightarrow 4(5)$ processes in leading order and matched with parton showers using Pythia (values in parenthesis are given for inclusive top anti-top pair production). QCD multijet events were produced in leading order using Pythia. All events were passed through the full simulation of the

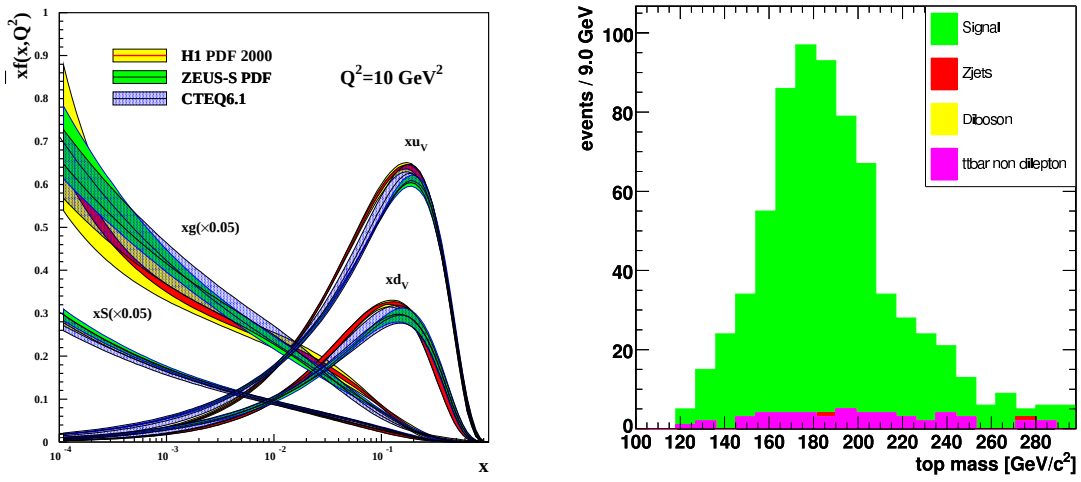

Fig. 23: (Left) Parton distribution functions (PDFs) from the HERA experiments H1 and ZEUS and from the CTEQ collaboration at a scale of $Q^2 = 10\,\mathrm{GeV}^2$. Of relevance for top quark production at the LHC are the gluon density functions at values $x > 0.01$ of the fractional proton momentum x. (Right) Top mass reconstructed from top anti-top quark pairs in the di-leptonic decay channel as expected from full simulation with the CMS detector with $1\,\mathrm{fb}^{-1}$ of integrated luminosity.

CMS detector including a simulation of the CMS L1 and High-Level-Trigger and mis-alignment and mis-calibration of the track detector and calorimeters as expected for the first $10\,\mathrm{pb}^{-1}$ were taken into account. Top events are selected by requiring a single isolated muon with transverse momentum $p_\mathrm{T} > 30\,\mathrm{GeV}$ in the pseudo-rapidity range of $|\eta| < 2.1$, a leading jet with calibrated $p_\mathrm{T} > 65\,\mathrm{GeV}$ and at least three further jets with calibrated $p_\mathrm{T} > 30\,\mathrm{GeV}$ in a pseudo-rapidity range of $|\eta| < 2.4$ in addition to the trigger criteria. With this selection the trigger efficiency is estimated to be above 90%. The muon is considered isolated if the summed p_T of all reconstructed tracks within a cone of $\Delta R = \sqrt{\Delta\phi^2 + \Delta\eta^2} < 0.3$ in the vicinity of the muon does not exceed $3\,\mathrm{GeV}$ and the summed calorimeter entries in the same area do not exceed $1\,\mathrm{GeV}$. Either b-tag information nor information on missing transverse energy are taken into consideration for the sake of a more robust event selection. In addition any of the selected jets is required to be seperated from the isolated muon by at least 0.3 units in ΔR.

This selection leads to a total of 128 events with top anti-top quark pairs in the semi-leptonic decay channel with a muon in the final state (with an estimated overall efficiency of 10%), 25 events with top anti-top pairs in other decay modes, 45 W+jets events, 7 Z+jets events and 11 multijet QCD events. The S/B is estmiated to be $1.5:1$ and the $S/B(QCD)$ is estimated to be $11:1$ with large uncertainties. As it is clear that the background from QCD multijet events will be the most difficult to control and to model methods for its estimation from data are discussed. This is a process still ongoing within the collaboration.

5.3 First measurements of the top mass

As an example for a measurement of the top quark mass within first data a study in the di-leptonic decay channel with $1\mathrm{fb}^{-1}$ of data taken with the CMS detector is presented [59]. Due to its clear event topology this channel is expected to have the best signal to background ratio. Main backgrounds are considered to be Z and di-boson production associated with additional hard jets and top events from other decay channels. All events were produced with the Pythia event generator in leading order and passed through the full simulation of the CMS detector including a simulation of the CMS L1 and High-Level-Trigger. Top events are selected by requiring two isolated leptons (e or μ) of opposite sign with transverse momentum $p_\mathrm{T} > 20\,\mathrm{GeV}$, two jets with $p_\mathrm{T} > 30\,\mathrm{GeV}$ and missing transverse momentum larger than $40\,\mathrm{GeV}$, in addition to the trigger criteria. Leptons are considered isolated if the summed p_T of all reconstructed tracks within a cone of $\Delta R = \sqrt{\Delta\phi^2 + \Delta\eta^2} < 0.2$ in the vicinity of the lepton does not exceed 10% of the lepton's momentum. Electrons are identified using a likelihood method exploiting shower shape characteristics and the matching of tracks and calorimeter objects. For leptons of the same type an additional veto on the Z invariant mass is implied. The jets are required to fulfill a b-tag requirement based on the p_T and the invariant mass of the associated tracks and the result of a combined b-tag algorithm [60]. This selection is expected to provide a signal over background ratio of $12:1$ for a top mass estimate between 100 and $300\,\mathrm{GeV}$ the remaining background mostly originating from other top decay channels. In fig. 23 (right) the most likely top mass determined from a parameter scan in the range of $(100\text{-}300)\,\mathrm{GeV}$ is shown. Unknowns are reduced imposing constraints on momentum conservation in the transverse plane, the W invariant mass and the equality of the top mass in both decay branches. Remaining ambiguities are taken into account by a weighting procedure based on the SM expectation of the neutrino

momentum spectrum. The fit of a Gaussian function yields a top mass of $m_{\rm top}^{\rm rec} = 178.5 \pm 1.5\,(\rm stat.) \pm 4\,(\rm syst.)\,\rm GeV$ for an input mass of $m_{\rm top}^{\rm gen} = 175\,\rm GeV$. Systematic uncertainties are expected to be dominated by the uncertainty of the validity of the imposed constraints in the presence of initial and final state radiation, and the uncertainty of the jet energy scale (JES). For $10\,\rm fb^{-1}$ the uncertainties are expected to be reduced to $\Delta m_{\rm top} = 0.5\,(\rm stat.) \pm 1\,(\rm syst.)\,\rm GeV$.

References

[1] Z. Lin and M. Gyulassy, Phys. Rev. **C51**, 2177 (1995).

[2] Y. Dokshitzer and D. Kharzeev, Phys. Lett. **B519**, 199 (2001).

[3] M. Djordjevic, M. Gyulassy, and S. Wicks, Phys. Rev. Lett. **94**, 112301 (2005).

[4] PHENIX Collaboration, S. Adler *et al.*, Phys. Rev. Lett. **96**, 032301 (2006).

[5] PHENIX Collaboration, A. Adare *et al.*, Phys. Rev. Lett. **98**, 172301 (2007).

[6] STAR Collaboration, B. Abelev *et al.*, Phys. Rev. Lett. **98**, 192301 (2007).

[7] R. Vogt, Eur. Phys. J. Special Topics **155**, 213 (2008).

[8] STAR Collaboration, A. Mischke *et al.*, J. Phys. **G35**, 104117 (2008). ArXiv: 0804.4601.

[9] A. Mischke, Phys. Lett. B. in press. ArXiv: 0807.1309.

[10] M. Cacciari, P. Nason, and R. Vogt, Phys. Rev. Lett. **95**, 122001 (2005).

[11] ALICE Collaboration, A. Dainese *et al.*, J. Phys. **G35**, 044046 (2008).

[12] ALICE Collaboration, F. Carminati *et al.*, J. Phys. **G30**, 1517 (2005).

[13] ALICE Collaboration, B. Alessandro *et al.*, J. Phys. **G32**, 1295 (2006).

[14] Y. Dokshitzer and D. Kharzeev, Phys. Lett. **B519**, 199 (2001).

[15] N. Armesto, A. Dainese, C. Salgado, and U. Wiedemann, Phys. Rev. **D71**, 054027 (2005).

[16] M. Mangano, P. Nason, and G. Ridolfi, Nucl. Phys. **B373**, 295 (1992).

[17] ALICE Collaboration, E. Bruna *et al.*, Preprint **nucl-ex/0703005** (2007).

[18] S. Eidelmann and others [Particle Data Group Collaboration], Phys. Lett. **B592**, 1 (2004).

[19] T. Sjöstrand, P. Edén, C. Friberg, L. Lönnblad, G. Miu, S. Mrenna, and E. Norrbin, Computer Phys. Commun. **135**, 238 (2001).

[20] F. Antinori, A. Dainese, M. Lunardon, and R. Turrisi, ALICE Internal Note **033** (2006).

[21] A. Dainese and M. Masera, ALICE Internal Note **027** (2003).

[22] UA1 Collaboration, C. Albajar *et al.*, Phys. Lett. **B 213**, 405 (1988).

[23] P. Crochet, R. Guernane, A. Morsch, and E. Vercellin, ALICE Internal Note **018** (2005).

[24] J. Baines *et al.* hep-ph/0601164.

[25] M. Cacciari, M. Greco, and P. Nason, JHEP **9805**, 007 (1998).

[26] H. Jung, Computer Phys. Commun. **143**, 100 (2002).

[27] M. Bedjidian *et al.* hep-ex/0311048.

[28] CDF Collaboration, F. Acosta *et al.*, Phys. Rev. **D71**, 032001 (2005). hep-ex/0412071;
CDF Collaboration, F. Acosta *et al.*, Phys. Rev. Lett. **88**, 161802 (2002).

[29] A. D. Martin, R. G. Roberts, W. J. Stirling, and R. S. Thorne, Eur. Phys. J. **C4**, 463 (1998). hep-ph/9803445.

[30] A. D. Martin, R. G. Roberts, W. J. Stirling, and R. S. Thorne, Phys. Lett. **B531**, 216 (2002). hep-ph/0201127.

[31] CTEQ Collaboration, H. L. Lai *et al.*, Eur. Phys. J. **C12**, 375 (2000). hep-ph/9903282.

[32] J. Pumplin *et al.*, JHEP **07**, 012 (2002).

[33] ATLAS Collaboration, ATLAS TDR 15, CERN/LHCC 99-15 (1999).

[34] D. Emeliyanov *et al.*, ATL-DAQ-CONF-2007-031 (2007).

[35] P. Jussel *et al.*, ATL-PHYS-PUB-2007-003 (2007).

[36] S. George, ATL-DAQ-2004-004 (2004).

[37] CDF Collaboration, F. Acosta *et al.*, Phys. Ref. **D71**, 032001 (2005).

[38] W. Yao *et al.*, J. of Phys. G **33**, 1 (2006).

[39] CDF Collaboration, F. Abe *et al.*, Phys. Rev. Lett. **69**, 3704 (1992).

[40] CDF Collaboration, F. Abulencia *et al.*, Phys. Rev. Lett. **99**, 132001 (2007).

[41] G. Bodwin, E. Braaten, and G. Lepage, Phys. Rev. **D51**, 1125 (1995).

[42] ATLAS Collaboration, CERN-OPEN-2008-020 (2008).

[43] CMS Collaboration, S. Chatrchyan *et al.*, JINST **3**, S08004 (2008).

[44] CMS Collaboration, CERN-LHCC-2006-021 (2006).

[45] CMS Collaboration, CERN-LHCC-2002-026 (2006).

[46] C. Weiser, CMS NOTE-2006/014 (2006).

[47] V. Andreev, D. Cline, and S. Otwinowski, CMS NOTE-2006/120 (2006).

[48] A. Buras, Phys. Lett. **B566**, 115 (2003).

[49] K. Babu and C. Kolda, Phys. Rev. Lett. **84**, 228 (2000).

[50] CDF Collaboration, T. Aaltonen *et al.*, Phys. Rev. Lett. **100**, 101802 (2008).

[51] CMS Collaboration, J. Layter *et al.*, CERN-LHCC-1997-032 (1997).

[52] U. Langenegger, CMS-CR-2006/071 (2006).

[53] M. Bona *et al.*, JHEP **0610**, 081 (2006).

[54] V. Ciulli *et al.*, CMS NOTE-2006/121 (2006).

[55] CDF Collaboration, Phys. Rev. Lett. **96**, 082002 (2006).

[56] X. Meng, J. Tao, and G. Chen, CMS NOTE-2006/118 (2006).

[57] M. Cacciari *et al.*, arXiv:0804.2008.

[58] CMS Collaboration, CMS PAS Top08-005.

[59] CMS Collaboration, J. Phys. **G34**, 995 (2007).

[60] R. Kinnunen and S. Lehti, CMS NOTE 2006/075.